Copy 214
RM L51C06

[redacted]

[redacted]

NACA

RESEARCH MEMORANDUM

AN INVESTIGATION OF A SUPERSONIC AIRCRAFT CONFIGURATION HAVING A TAPERED WING WITH CIRCULAR-ARC SECTION AND 40° SWEEPBACK

A PRESSURE-DISTRIBUTION STUDY OF THE AERODYNAMIC CHARACTERISTICS OF THE WING AT MACH NUMBER 1.40

By Norman F. Smith, Julian H. Kainer,
and Robert A. Webster

Langley Aeronautical Laboratory
Langley Field, Va.

[redacted]

NATIONAL ADVISORY COMMITTEE
FOR AERONAUTICS

WASHINGTON
April 20, 1951

[redacted]

[redacted]

Classification cancelled (or changed to Unclassified)

By Authority of NASA Tech Pub Announcement # [illegible]
(OFFICER AUTHORIZED TO CHANGE)

By 28 Jun 58
NAME AND

[illegible]
GRADE OF OFFICER MAKING CHANGE)

24 Mar 61
DATE

NATIONAL ADVISORY COMMITTEE FOR AERONAUTICS

RESEARCH MEMORANDUM

AN INVESTIGATION OF A SUPERSONIC AIRCRAFT CONFIGURATION HAVING A TAPERED WING WITH CIRCULAR-ARC SECTION AND 40° SWEEPBACK

A PRESSURE-DISTRIBUTION STUDY OF THE AERODYNAMIC CHARACTERISTICS OF THE WING AT MACH NUMBER 1.40

By Norman F. Smith, Julian H. Kainer, and Robert A. Webster

SUMMARY

A pressure-distribution investigation of the wing, in the presence of the fuselage, of a supersonic aircraft configuration has been conducted in the Langley 4- by 4-foot supersonic tunnel at a Mach number of 1.40 and a Reynolds number, based on the mean aerodynamic chord, of 0.598×10^6. The quarter chord of the wing was swept back 40°; the wing had an aspect ratio of 4, a taper ratio of 0.5, and 10-percent-thick circular-arc sections perpendicular to the quarter-chord line. For the Mach number of the present investigation, the wing had supersonic leading and trailing edges; the leading edge, however, had a detached shock wave throughout the angle-of-attack range.

The results of this investigation have been compared with the results of a previously reported investigation of the same configuration in the 4- by 4-foot supersonic tunnel at a Mach number of 1.59 and Reynolds number, based on the mean aerodynamic chord, of 0.575×10^6. In general, the agreement between the experimental and the theoretical wing characteristics at Mach number 1.40 was not as good as at Mach number 1.59. The nature of the flow for both Mach numbers 1.40 and 1.59 was qualitatively similar. The experimental lift and drag coefficients decreased and the pitching moments became more stable with increasing Mach number, as predicted by linear theory. For both Mach numbers, the experimental lift and drag coefficients and the stability were less

than predicted by linear theory. The discrepancies resulted principally from the existence of large regions of separated flow at the trailing edge and at the outboard stations of the wing and in part from the pressure of a detached leading-edge shock.

At both Mach numbers a pronounced interference of the fuselage on the wing was observed at the inboard stations but this effect diminished fairly rapidly outboard.

INTRODUCTION

A comprehensive investigation of a supersonic aircraft configuration having a tapered wing of circular-arc section, aspect ratio 4, and 40° sweepback of the quarter-chord line has been conducted in the Langley 4- by 4-foot supersonic tunnel. In order to obtain a detailed knowledge of the flow over the model as well as the general aerodynamic characteristics, extensive tests were conducted on both a large-scale force model and a pressure model of the complete configuration at Mach numbers of 1.40 and 1.59. The results of the pressure-distribution study of the fuselage and its canopies are reported in references 1 and 2 at Mach numbers of 1.40 and 1.59, respectively. The results of the pressure-distribution study of the wing obtained during tests of the complete pressure model at a Mach number of 1.59 are presented in reference 3. The force-model investigations of static longitudinal and lateral stability characteristics at Mach numbers of 1.40 and 1.59 are presented in references 4 to 6.

This report presents the results of the pressure-distribution study of the wing obtained during tests of the complete pressure model at a Mach number of 1.40 and a Reynolds number, based on the mean aerodynamic chord, of 0.598×10^6. For this investigation, the component of Mach number normal to the leading and trailing edges was supersonic; however, the shock wave at the leading edge remained detached throughout the angle-of-attack range. The pressure data have been analyzed in terms of section and over-all wing characteristics, and the experimental results have been compared with the corresponding calculations based on linear theory and with some experimental and theoretical results at a Mach number of 1.59 (reference 3).

SYMBOLS

Free-stream conditions:

ρ	mass density of air
V	airspeed
a	speed of sound in air
M	Mach number (V/a)
q	dynamic pressure $\left(\frac{1}{2}\rho V^2\right)$
p	static pressure

Wing geometry:

S	area extended through the fuselage
b	span
A	aspect ratio (b^2/S)
c	airfoil chord at any spanwise station
c'	mean aerodynamic chord $\left(\frac{2}{S}\int_0^{b/2} c^2 dy\right)$
$\bar{c}$	mean chord (S/b)
x	chordwise distance measured streamwise from the airfoil leading edge
y	spanwise distance measured from the plane of symmetry of the wing
z	normal distance measured from the airfoil chord line
α	angle of attack of the wing, degrees

Pressure data:

p_l	local static pressure

P pressure coefficient $\left(\frac{p_l - p}{q}\right)$

c_n section normal-force coefficient $\left[\int_0^1 (P_{L'} - P_U)\,d\left(\frac{x}{c}\right)\right]$

c_c section chord-pressure-force coefficient

$$\left\{\int_0^1 \left[\left(P\frac{dz}{dx}\right)_U - \left(P\frac{dz}{dx}\right)_{L'}\right] d\left(\frac{x}{c}\right)\right\}.$$

c_l section lift coefficient $(c_n \cos\alpha - c_c \sin\alpha)$

c_d section pressure-drag coefficient $(c_n \sin\alpha + c_c \cos\alpha)$

c_m section pitching-moment coefficient, due to normal forces, about the 25-percent position of the airfoil chord

$$\left[\int_0^1 (P_{L'} - P_U)\left(0.25 - \frac{x}{c}\right)d\left(\frac{x}{c}\right)\right]$$

$c_{m_{x_1}}$ section pitching-moment coefficient, due to normal forces, about a line perpendicular to the plane of symmetry and passing through the 25-percent position of the mean aerodynamic chord $\left[\int_0^1 (P_{L'} - P_U)\left(\frac{x_1}{c} - \frac{x}{c}\right)d\left(\frac{x}{c}\right)\right]$

x_1 distance from the leading edge of each spanwise station to a line perpendicular to the plane of symmetry and passing through the 25-percent position of the mean aerodynamic chord (positive rearward from leading edge)

C_L wing lift coefficient $\left(C_L = \int_0^1 c_l \frac{c}{\bar{c}}\, d\left(\frac{y}{b/2}\right) = \frac{\text{Lift}}{qS}\right)$

C_D wing pressure-drag coefficient

$$\left(C_D = \int_0^1 c_d \frac{c}{\bar{c}} \, d\left(\frac{y}{b/2}\right) = \frac{\text{Drag}}{qS}\right)$$

C_m wing pitching-moment coefficient about a line perpendicular to the plane of symmetry and passing through the 25-percent position of the mean aerodynamic chord

$$\left(C_m = \frac{\bar{c}}{c'} \int_0^1 \frac{c_{m_{x_1}} c^2}{(\bar{c})^2} \, d\left(\frac{y}{b/2}\right) = \frac{\text{Pitching moment}}{qSc'}\right)$$

$\frac{y_{cp}}{b/2}$ spanwise location of the center of pressure of the normal force $\left(\int_0^1 \frac{c_n c}{\bar{c}} \frac{y}{b/2} \, d\left(\frac{y}{b/2}\right) \Big/ \int_0^1 \frac{c_n c}{\bar{c}} \, d\left(\frac{y}{b/2}\right)\right)$

n_o chordwise location of the wing aerodynamic center

$$\left(0.25 - \frac{\partial C_m}{\partial C_L}\right)$$

Subscripts:

L' lower surface

U upper surface

α value at angle of attack

$\alpha = 0$ value at 0° angle of attack

APPARATUS

The Langley 4- by 4-foot supersonic tunnel is a rectangular, closed-throat, single-return wing tunnel designed for a nominal Mach number range from 1.2 to 2.2. Detailed descriptions of the tunnel and calibration of the test section are presented in references 1 and 2. The details of the wing and model (figs. 1 to 4) are discussed in reference 3.

TESTS, CORRECTIONS, AND ACCURACY

The basic pressure data over the wing were obtained for angles of attack of -2°, 0°, 1°, 3°, 5°, 7°, 9°, 11°, and 13° at a Mach number of 1.40 and a Reynolds number, based on the mean aerodynamic chord, of 0.598×10^6. The aerodynamic data have been obtained at the following tunnel stagnation conditions: pressure, 0.25 atmosphere; temperature, 110° F; and dew point, -30° F. For these test conditions, the calibration data (reference 1) of the test section indicate that the effects of condensation on the flow over the model are probably extremely small. Since the magnitudes of the flow angle, Mach number, and pressure gradients are small in the vicinity of the model, no corrections due to these sources have been applied to the data. A discussion of the accuracy of the wing data is presented in reference 3.

PRESENTATION OF RESULTS

The basic pressure data were obtained during tests of the complete model at four spanwise stations parallel to the stream and at two stations oblique to the stream. (See fig. 3.) The pressure distributions from the streamwise orifices are presented in figure 5 and table I and from the oblique orifices in figure 6 and table II. In all the figures, flagged symbols are faired with dashed lines to designate the lower-surface data. A comparison of the basic pressure data for Mach numbers of 1.40 and 1.59 (reference 3) at angles of attack of 3° and 11° is presented for the four streamwise stations in figure 7. The unit chordwise-pressure-force coefficient, defined as the product of the local pressure coefficient and the local slope in the streamwise direction, is presented in figure 8 for the four streamwise stations for representative angles of attack of -2°, 0°, 5°, and 13°.

The pressure data of figure 5 are compared with calculations based on linear theory for zero angle of attack in figure 9 and for several angles of attack in figure 10. The theoretical calculations were obtained by means of references 7 to 10 as explained in reference 3.

The section normal-force, chord-pressure-force, and pitching-moment coefficients at the four spanwise stations obtained by integrating the pressure data of figures 5 and 8, and the section lift and pressure-drag coefficients obtained from a resolution of the section normal-force and chord-pressure-force coefficients are presented in figure 11. In addition, figure 11 contains similar data at Mach number 1.59 (from reference 3) and the corresponding theoretical calculations for both Mach numbers. Since the effects of skin friction are not included in the drag coefficients obtained from the integrated pressure data, the experimental and theoretical drag coefficients are on a comparable basis. The spanwise distribution of the section coefficients and load parameters for normal force, drag, and pitching moment are presented in figures 12 to 14. Although the theoretical results for all conditions in figures 12 to 14 may be obtained from figure 11, only one representative theoretical curve has been presented therein. In figure 14, the section pitching-moment coefficients have been referenced to the quarter-chord line of the individual sections, and the loading parameters have been referenced to a line which is perpendicular to the plane of symmetry of the model and passes through the 25-percent position of the mean aerodynamic chord. A comparison of the experimental and theoretical load parameters for the section normal-force, drag, and pitching-moment coefficients for Mach numbers of 1.40 and 1.59 (reference 3) at angles of attack of 3° and 11° is presented in figure 15. Figure 16 presents a comparison of the experimental and theoretical locations of the centers of pressure of the normal forces at the four spanwise stations.

The over-all experimental and theoretical wing characteristics for both $M = 1.40$ and 1.59 (reference 3), obtained from integration of the spanwise distributions, are presented in figure 17 as a function of angle of attack. These results were calculated by extrapolating the data from the wing-fuselage juncture to the center line of the model; the coefficients thus obtained are more nearly equivalent to a wing-alone configuration than to a wing-body combination. (See reference 3.) Figure 18 presents the experimental and theoretical wing lift-drag ratios (obtained from fig. 17) for Mach numbers of 1.40 and 1.59 (reference 3). Figure 19 presents a comparison of the experimental and theoretical location of the lateral center of pressure $\frac{y_{cp}}{b/2}$, and the aerodynamic center n_o to indicate quantitatively the accuracy with which the root bending moments and the margin of static stability of the wing can be predicted.

DISCUSSION

A detailed discussion of the limitations of experimental and theoretical comparisons is contained in reference 3. In general, the basic pressure data for $M = 1.40$ indicate flow characteristics which are similar to those observed at $M = 1.59$ and which are discussed at length in reference 3. The discussion in the present report will therefore be abbreviated in this respect, but will treat in detail comparisons of the data and theory for the Mach numbers of 1.40 and 1.59.

Leading-edge pressure peaks induced by the detached leading-edge shock wave first appear with increasing angle of attack under approximately the same conditions for both Mach numbers, that is, at $\alpha = 5^{\circ}$ for $\frac{y}{b/2} = 0.186$ and 0.436 and at $\alpha = 3^{\circ}$ for $\frac{y}{b/2} = 0.686$ and 0.937 (figs. 5 and 7 herein, and fig. 5, reference 3). Although the component of Mach number normal to the leading edge is supersonic for both Mach numbers, the leading-edge shock is detached since the leading-edge wedge angle exceeds the maximum allowable for an attached shock.

The wing-body interference effects at $M = 1.40$ for $\alpha = 0^{\circ}$ (fig. 9) are similar to the effects obtained at $M = 1.59$ (reference 3). The pressures on the upper surface have higher positive (or lower negative) values than those on the lower surface in the vicinity of the root section; this effect diminishes outboard.

Some interference effects at the trailing edge in the form of sudden pressure increases are observed at all stations for $M = 1.40$ (figs. 5 and 6). These effects are stronger near the root section for the complete angle-of-attack range and diminish spanwise. Similar pressure increases were observed near the wing trailing edge at the inboard station at $M = 1.59$. These effects were restricted to the inboard station at this Mach number (fig. 7), probably because the zone of influence of the fuselage at $M = 1.59$ did not extend outboard of the root section.

For zero angle of attack, a build-up of laminar separation from about the rear 15 percent of the chord at the root to about the rear 30 percent of the chord at the tip is indicated in the data of figure 9. Comparison of these data with corresponding data at $M = 1.59$ (reference 3) indicates approximately the same point of separation.

Examination of the lifting-pressure data for each spanwise station (fig. 10) indicates slightly more lift on the expansion surface as observed for $M = 1.59$ (reference 3). While all the stations at

$M = 1.59$ exhibit less lift than predicted, the tip station at $M = 1.40$ (fig. 10) indicates more lift than predicted. The marked contrast between the predicted and experimental flow is due to the effects of the detached shock wave and flow separation, which cannot be included in linear theory.

The section data for Mach numbers of 1.40 and 1.59 are compared in figure 11. At $M = 1.40$, the lift coefficients are less and the pitching moments are less stable than the predicted values for all stations except the tip station, whereas the drag coefficients are less than the predicted values for all stations. At the tip station, the predicted lifting pressures are lower than the measured pressures (fig. 10) which causes section lift coefficients to be greater than predicted. The predicted pitching-moment coefficients are less stable since the predicted centers of pressure at the tip station are forward of the experimental positions. As the Mach number is increased from 1.40 to 1.59, the experimental lift and drag coefficients decrease and the pitching-moment coefficients become more stable, as predicted by linear theory.

The spanwise plots of the section data (figs. 12 to 14) clearly indicate that the measured lift, drag, and pitching-moment coefficients are less than predicted for all stations except the tip station. In figure 14, a positive loop in the theoretical curve for C_m is observed in the vicinity of the tip which is a direct consequence of the interaction of the root and tip Mach cones and the reflection of the root Mach cone off the wing tip (see figs. 3 and 10); however, these effects of the linear theory do not occur in the experimental data because of the presence of the detached shock and the separation effects. It may be noted that such effects were not found in the theory for $M = 1.59$ (reference 3) since, for practical purposes, the Mach cone from the root did not reflect off the wing tip. Hence, the calculated lift, drag, and pitching-moment coefficients were greater than the measured values for all stations including the tip station. Furthermore, the predicted qualitative trends agree well for both Mach numbers except the one for the tip station at $M = 1.40$.

A comparison of the spanwise distribution of load, drag, and pitching-moment parameters (fig. 15) at two angles of attack for Mach numbers of 1.40 and 1.59 shows the decreasing trends with increasing Mach number predicted by linear theory.

The data of figure 16 show that the experimental centers of pressure are forward of the theoretical locations. Very little shift in the measured center-of-pressure location is observed either spanwise or with angle of attack.

The integrated results show a decrease in lift, drag, and pitching-moment coefficients with increasing Mach number for all angles of attack (fig. 17) as predicted by linear theory. Closer agreement between experiment and theory is observed, however, for $M = 1.59$ since the flow conditions more nearly approach the assumptions required by linear theory.

At a Mach number of 1.40 the maximum experimental L/D was 5.6 as compared with the predicted value of 4.4. (See fig. 18.) Better agreement was observed at $M = 1.59$, and a higher maximum L/D was realized at $M = 1.40$ than at $M = 1.59$. These phenomena are a consequence of the fact that, in the vicinity of transonic flows, the actual drag does not follow the predicted asymptotic peaks while the actual lifts do follow such a trend.

For a Mach number of 1.40 the measured aerodynamic center was forward of the predicted location, while excellent agreement was observed for the lateral center of pressure for all angles of attack (fig. 19). This agreement may be somewhat fortuitous in that the integrated result is affected by the disagreement in the section lifts in the vicinity of the wing tip at $M = 1.40$ (fig. 10). Comparison of these data with the results of reference 3 shows that a decrease in Mach number from 1.59 to 1.40 resulted in a forward movement of the aerodynamic center of about 5 percent of the chord and an outboard shift in the lateral center of pressure of about 5 percent of the wing semispan.

CONCLUDING REMARKS

A pressure-distribution investigation of the wing (in the presence of the fuselage) of a complete supersonic aircraft configuration has been conducted in the Langley 4- by 4-foot supersonic tunnel at a Mach number of 1.40 and a Reynolds number, based on the mean aerodynamic chord, of 0.598×10^6. The quarter chord of the wing was swept back 40°; the wing had an aspect ratio of 4, a taper ratio of 0.5, and 10-percent-thick circular-arc sections perpendicular to the quarter-chord line. For the Mach number of the present investigation, the wing had supersonic leading and trailing edges; the leading edge, however, had a detached shock wave throughout the angle-of-attack range.

The results of this investigation were compared with the results of an investigation of the same configuration in the 4- by 4-foot supersonic tunnel at a Mach number of 1.59 and a Reynolds number, based on the mean aerodynamic chord, of 0.575×10^6. In general, the agreement between the experimental and the theoretical wing characteristics at Mach number 1.40 was not as good as at Mach number 1.59. The nature of the flow for both Mach numbers 1.40 and 1.59 was qualitatively similar. The experimental lift and drag coefficients decreased and the pitching moments became more stable with increasing Mach number, as predicted by linear theory. For both Mach numbers, the experimental lift and drag coefficients and the stability were less than predicted by linear theory. The discrepancies resulted principally from the existence of large regions of separated flow at the trailing edge and at the outboard stations of the wing and in part from the pressure of a detached leading-edge shock.

At both Mach numbers a pronounced interference of the fuselage on the wing was observed at the inboard stations but this effect diminished fairly rapidly outboard.

Langley Aeronautical Laboratory
National Advisory Committee for Aeronautics
Langley Field, Va.

REFERENCES

1. Hasel, Lowell E., and Sinclair, Archibald R.: A Pressure-Distribution Investigation of a Supersonic-Aircraft Fuselage and Calibration of the Mach Number 1.40 Nozzle of the Langley 4- by 4-Foot Supersonic Tunnel. NACA RM L50B14a, 1950.

2. Cooper, Morton, Smith, Norman F., and Kainer, Julian H.: A Pressure-Distribution Investigation of a Supersonic Aircraft Fuselage and Calibration of the Mach Number 1.59 Nozzle of the Langley 4- by 4-Foot Supersonic Tunnel. NACA RM L9E27a, 1949.

3. Cooper, Morton, and Spearman, M. Leroy: An Investigation of a Supersonic Aircraft Configuration Having a Tapered Wing With Circular-Arc Section and 40° Sweepback. A Pressure Distribution Study of the Aerodynamic Characteristics of the Wings at Mach Number 1.59. NACA RM L50C24, 1950.

4. Spearman, M. Leroy: An Investigation of a Supersonic Aircraft Configuration Having a Tapered Wing with Circular-Arc Sections and 40° Sweepback. Static Longitudinal Stability and Control Characteristics at a Mach Number of 1.40. NACA RM L9L08, 1950.

5. Spearman, M. Leroy, and Hilton, John H., Jr.: An Investigation of a Supersonic Aircraft Configuration Having a Tapered Wing with Circular-Arc Sections and 40° Sweepback. Static Longitudinal Stability and Control Characteristics at a Mach Number of 1.59. NACA RM L50E12, 1950.

6. Spearman, M. Leroy: An Investigation of a Supersonic Aircraft Configuration Having a Tapered Wing with Circular-Arc Sections and 40° Sweepback. Static Lateral Stability Characteristics at Mach Numbers of 1.40 and 1.59. NACA RM L50C17, 1950.

7. Jones, Robert T.: Thin Oblique Airfoils at Supersonic Speed. NACA Rep. 851, 1946.

8. Kainer, Julian H.: Theoretical Calculations of the Supersonic Pressure Distribution and Wave Drag for a Limited Family of Tapered Sweptback Wings with Symmetrical Parabolic-Arc Sections at Zero Lift. NACA TN 2009, 1949.

9. Puckett, Allen E.: Supersonic Wave Drag of Thin Airfoils. Jour. Aero. Sci., vol. 13, no. 9, Sept. 1946, pp. 475-484.

10. Evvard, John C.: Distribution of Wave Drag and Lift in the Vicinity of Wing Tips at Supersonic Speeds. NACA TN 1382, 1947.

TABLE I.- PRESSURE COEFFICIENT DATA FOR FOUR SPANWISE STATIONS

(a) $\frac{y}{b/2} = 0.186$

Orifice station (percent c)	Pressure coefficient								
	$\alpha = -2^\circ$	$\alpha = 0^\circ$	$\alpha = 1^\circ$	$\alpha = 3^\circ$	$\alpha = 5^\circ$	$\alpha = 7^\circ$	$\alpha = 9^\circ$	$\alpha = 11^\circ$	$\alpha = 13^\circ$
Upper surface									
1.020	0.513	0.400	0.334	0.143	-0.084	-0.294	-0.408	-0.490	
2.549	.416	.318	.270	.141	0	-.212	-.350	-.458	-0.528
4.971	.348	.263	.226	.125	.024	-.101	-.255		
7.521	.294	.217	.180	.097	.016	-.053	-.161	-.323	-.387
9.943	.268	.197	.164	.089	.012	-.055	-.135	-.251	-.363
11.727	.236	.171	.139	.071	-.004	-.075		-.237	-.375
13.512				.065	-.008				
19.885	.129	.064	.037	-.019	-.082	-.132	-.189	-.233	-.325
25.876	.083	.016	-.011	-.067	-.128	-.180	-.231	-.279	-.345
40.790	.015	-.045	-.071	-.127	-.180	-.226	-.271	-.315	-.365
50.988	-.005	-.063	-.087	-.143	-.188	-.232	-.271	-.309	-.355
60.293	-.041	-.089	-.110	-.161	-.200	-.236	-.271	-.303	-.343
72.020	-.102	-.144	-.162	-.207	-.244	-.272	-.300	-.325	-.355
82.473	-.160	-.196	-.212	-.247	-.282	-.308	-.332	-.354	-.375
89.484	-.188	-.216	-.212	-.225	-.308	-.332	-.352	-.372	-.395
97.132	-.152	-.180	-.180	-.209	-.248	-.204	-.205	-.205	-.283
Lower surface									
2.040	0.001	0.173	0.234	0.325	0.403	0.471	0.535	0.595	0.642
6.119	.059	.126	.164	.225	.292	.358	.425	.490	.543
11.090	.011	.074	.105	.161	.232	.296	.358	.419	.475
15.041	-.003	.056	.085	.145	.206	.264	.322	.385	.455
18.228	-.009	.046	.077	.129	.188	.242	.298	.371	.439
23.072	-.023	.026	.053	.101	.154	.206	.272	.347	.412
29.955	-.039	.007	.015	.057	.110	.190	.237	.325	.376
36.584		-.037	-.011	.033	.086	.149	.217	.285	.348
46.526	-.095	-.049	-.027	.015	.066	.123	.181	.242	.296
55.959	-.120	-.079	-.059	-.017	.030	.083	.137	.198	.253
66.794	-.156	-.119	-.099	-.059	-.016	.031	.081	.136	.183
76.864	-.204	-.168	-.150	-.115	-.074	-.029	.018	.071	.114
84.895	-.244	-.206	-.186	-.157	-.116	-.073	-.026	.023	.066
91.396	-.264	-.198	-.200	-.179	-.138	-.097	-.050		.040
97.387	-.234	-.176	-.180	-.203	-.128	-.120	-.090	-.042	-.005

NACA

TABLE I.- PRESSURE COEFFICIENT DATA FOR FOUR SPANWISE STATIONS - Continued

(b) $\frac{y}{b/2} = 0.436$

Orifice station (percent c)	Pressure coefficient								
	$\alpha = -2^{o}$	$\alpha = 0^{o}$	$\alpha = 1^{o}$	$\alpha = 3^{o}$	$\alpha = 5^{o}$	$\alpha = 7^{o}$	$\alpha = 9^{o}$	$\alpha = 11^{o}$	$\alpha = 13^{o}$
Upper surface									
5.477	0.374	0.288	0.230	0.119	-0.116	-0.302	-0.414	-0.496	-0.551
20.429	.200	.142	.101	.031	-.026		-.293	-.372	-.458
26.351	.133	.078	.039	-.023	-.068	-.118	-.295	-.378	-.456
30.348	.083	.030	-.009	-.069	-.114	-.146	-.293	-.388	-.456
33.309	.053	-.001	-.037	-.097	-.146	-.174	-.289	-.388	-.456
40.266	.005	-.045	-.085	-.145	-.192	-.228	-.281	-.400	-.464
46.780	-.031	-.081	-.116	-.177	-.224	-.266	-.300	-.410	-.476
51.369	-.035	-.089	-.122	-.185				-.372	-.432
60.992	-.099	-.142	-.176	-.233	-.280	-.324	-.360	-.404	-.488
67.358	-.122	-.160	-.194	-.249	-.294	-.338	-.380	-.416	-.490
77.276	-.172	-.206	-.232	-.281	-.318	-.362	-.408	-.438	-.480
85.270	-.218	-.236	-.220	-.303	-.350	-.385	-.428	-.436	-.476
90.007	-.214	-.210	-.208	-.303	-.366	-.377	-.376	-.345	-.432
97.557	-.190	-.198	-.208	-.275	-.252	-.220	-.241	-.267	-.371
Lower surface									
3.553	0.067	0.257	0.308	0.411	0.491	0.559	0.618	0.673	0.729
7.254	.101	.199	.246	.333	.413	.483	.551	.601	.664
11.695	.083	.173	.222	.285	.357	.421	.487	.534	.604
22.650	.003	.079	.101	.159	.224	.288	.352	.407	.471
31.236	-.055	.009	.027	.083	.152	.218	.276	.327	.398
34.493	-.083	-.019	.001	.055	.126	.190	.244	.299	.368
48.409	-.158	-.097	-.077	-.023	.040	.097	.149	.204	.267
55.366	-.190	-.128	-.108	-.057	.002	.053	.109	.160	.219
63.360	-.216	-.160	-.140	-.097	-.042	.009	.061	.111	.163
71.799	-.250	-.200	-.184	-.143	-.088	-.039	.006	.051	.104
79.349	-.270	-.224	-.212	-.177	-.126	-.081	-.040	.003	.052
86.751	-.306	-.208	-.240	-.215	-.170	-.128	-.088	-.046	.001
92.228	-.328	-.196	-.216	-.233	-.190	-.160	-.121	-.082	-.033
96.817	-.274	-.206	-.208	-.207	-.180	-.190	-.153	-.114	-.075

NACA

[redacted]

TABLE I.- PRESSURE COEFFICIENT DATA FOR FOUR SPANWISE STATIONS - Continued

(c) $\frac{y}{b/2} = 0.686$

Orifice station (percent c)	Pressure coefficient								
	$\alpha = -2^\circ$	$\alpha = 0^\circ$	$\alpha = 1^\circ$	$\alpha = 3^\circ$	$\alpha = 5^\circ$	$\alpha = 7^\circ$	$\alpha = 9^\circ$	$\alpha = 11^\circ$	$\alpha = 13^\circ$
Upper surface									
2.476	0.475	0.356	0.262	-0.061	-0.304	-0.430	-0.501	-0.539	-0.567
10.080	.314	.241	.190		-.156	-.291	-.396	-.468	-.528
13.439	.268	.205	.155	.069	-.130	-.267	-.378	-.450	-.506
20.159	.204	.146	.107	.035	-.074	-.223	-.310	-.373	-.424
25.995	.137	.080	.043	-.023	-.062			-.369	-.420
33.245	.061	.007		-.093	-.126	-.279	-.358	-.424	-.480
39.965	.017	-.039	-.075	-.137	-.172	-.291	-.368	-.432	-.484
46.508	-.015	-.069	-.104	-.163	-.200				
50.928	-.059	-.105	-.144	-.201	-.238	-.316	-.398	-.456	-.500
55.880	-.083	-.128	-.168	-.223	-.262	-.314	-.406	-.460	-.494
66.844	-.146	-.184	-.220	-.275	-.310	-.340	-.434	-.482	-.484
72.325	-.178	-.216	-.248	-.301	-.338	-.366	-.452	-.484	-.476
79.929	-.222	-.256	-.266	-.339	-.374	-.402	-.456	-.462	-.460
84.881	-.250	-.252	-.240	-.361	-.396	-.424	-.436	-.460	-.458
90.186	-.270	-.224	-.228	-.374	-.404	-.408	-.424	-.446	-.452
97.259	-.264	-.224	-.232	-.331	-.328	-.336	-.412	-.432	-.458
Lower surface									
2.476	0.057	0.292	0.362	0.468	0.553	0.612	0.668	0.715	0.751
7.427	.089	.219	.267	.353	.429	.491	.551	.604	.656
11.848	.085	.189	.222	.295	.365	.425	.485	.539	.596
16.446	.049	.142	.170	.237	.306	.364	.423	.479	.535
30.062	-.047	.022	.047	.105	.174	.233	.292	.350	.406
36.428	-.091	-.021	-.001	.055	.124	.177	.237	.294	.350
42.971	-.126	-.061	-.043	.013	.082	.133	.191	.249	.302
48.806	-.162	-.101	-.081	-.027	.038	.089	.145	.203	.257
53.581	-.188	-.127	-.108	-.053	.008	.056	.113	.167	.219
58.179	-.214	-.154	-.136	-.083	-.026	.024	.079	.132	.185
63.837	-.244	-.184	-.164	-.115	-.060	-.014	.042	.094	.146
69.850	-.272	-.216	-.196	-.151	-.096	-.050	.006	.054	.108
76.923	-.306	-.248	-.232	-.189	-.136	-.094	-.042	.005	.056
82.582	-.320	-.254	-.252	-.213	-.166	-.121	-.074	-.027	.020
87.533			-.268	-.243	-.194	-.151	-.106	-.059	-.011
93.015	-.356	-.224	-.244	-.267	-.218	-.177	-.133	-.087	-.039
97.436	-.306	-.224	-.234	-.281	-.256				-.101

NACA

TABLE I.- PRESSURE COEFFICIENT DATA FOR FOUR SPANWISE STATIONS - Concluded

(d) $\frac{y}{b/2} = 0.937$

Orifice station (precent c)	Pressure coefficient								
	$\alpha = -2^{\circ}$	$\alpha = 0^{\circ}$	$\alpha = 1^{\circ}$	$\alpha = 3^{\circ}$	$\alpha = 5^{\circ}$	$\alpha = 7^{\circ}$	$\alpha = 9^{\circ}$	$\alpha = 11^{\circ}$	$\alpha = 13^{\circ}$
Upper surface									
2.420	0.497	0.364	0.260	-0.075	-0.322	-0.413	-0.474	-0.511	-0.528
13.641	.264	.187	.135	.051	-.178	-.290	-.386	-.472	-.530
20.242	.186	.120	.077	.005	-.170	-.274	-.364	-.434	-.494
30.363	.057	.014	-.019	-.063	-.178	-.274	-.364	-.428	-.484
33.223	.023	-.013	-.043	-.083	-.180	-.274	-.358	-.424	-.476
36.744	-.013	-.045	-.073	-.111	-.186	-.282	-.356	-.420	-.470
40.264	-.037	-.065	-.091	-.129	-.184	-.278	-.344	-.404	-.444
46.865	-.091	-.113	-.141	-.177	-.200	-.310	-.376	-.436	-.476
60.946	-.162	-.180	-.204	-.237	-.244	-.346	-.406	-.458	-.484
67.327	-.198	-.214	-.236	-.269	-.274	-.369	-.428	-.476	-.496
85.369	-.290	-.216	-.220	-.347	-.358	-.423	-.468	-.492	-.492
92.629	-.310	-.210	-.216	-.363	-.378	-.421	-.460	-.492	-.490
98.350	-.264	-.208	-.212	-.299	-.314	-.362	-.420	-.456	-.460
Lower surface									
2.860	0.019	0.281	0.356	0.472	0.557	0.622	0.668	0.711	0.749
7.701	.095	.233	.282	.367	.441	.501	.555	.608	.654
12.321	.081	.189	.228	.305	.375	.437	.489	.541	.588
16.722	.073	.157	.190	.259	.328	.388	.435	.485	.531
23.322	.001	.078	.063	.163	.226	.280	.328	.378	.425
28.383	-.039	.018	.039	.089	.150	.204	.248	.298	.350
31.903	-.059	-.007	.007	.049	.106	.159	.207	.257	.306
38.504	-.102	-.057	-.043	-.009	.038	.087	.129	.179	.227
43.564	-.112	-.049	-.043	-.037	.006	.047	.083	.136	.171
49.505	-.170	-.128	-.118	-.091	-.058	-.011	.026	.072	.116
56.326	-.206	-.166	-.160	-.131	-.104	-.067	-.026	.016	.058
64.466	-.242	-.204	-.196	-.171	-.146	-.110	-.074	-.033	.005
88.009	-.318	-.210	-.220	-.289	-.272	-.246	-.221	-.188	-.156
93.729	-.296	-.208	-.216	-.305	-.292	-.270	-.249	-.220	-.186
98.350	-.270	-.208	-.212	-.291	-.308	-.326	-.324	-.303	-.277

TABLE II.- PRESSURE COEFFICIENT DATA FOR TWO OBLIQUE STATIONS

(a) Station A

Orifice station (percent c)	Pressure coefficient								
	$\alpha = -2^\circ$	$\alpha = 0^\circ$	$\alpha = 1^\circ$	$\alpha = 3^\circ$	$\alpha = 5^\circ$	$\alpha = 7^\circ$	$\alpha = 9^\circ$	$\alpha = 11^\circ$	$\alpha = 13^\circ$
Upper surface									
2.273	0.429	0.302	0.232	-0.005	-0.290	-0.403	-0.479	-0.528	-0.557
8.902	.300	.215	.164	.049	-.136	-.274	-.370	-.452	-.518
29.545	.067	.009	-.021	-.089	-.140	-.214	-.340	-.408	-.468
36.364	.013	-.045	-.071	-.135	-.186	-.224	-.344	-.414	-.468
46.970	-.051	-.103	-.130	-.189	-.242	-.280	-.326	-.424	-.474
63.068	-.148	-.194	-.216	-.264	-.312	-.352	-.392	-.432	-.498
80.114	-.220	-.252	-.234	-.316	-.352	-.381	-.444	-.444	-.474
93.939	-.212	-.208	-.210	-.328	-.308	-.248	-.237	-.252	-.275
Lower surface									
4.356	0.103	0.237	0.296	0.390	0.463	0.529	0.589	0.642	0.694
22.727	-.031	.032	.061	.119	.180	.250	.310	.370	.431
46.591	-.174	-.125	-.097	-.041	.016	.069	.133	.191	.245
56.250	-.228	-.176	-.150	-.097	-.048	.007	.062	.116	.169
73.295	-.280	-.242	-.222	-.181	-.136	-.085	-.038	.009	.058
87.879	-.240	-.214	-.238	-.217	-.188	-.146	-.104	-.059	-.013
96.402	-.238	-.204	-.208	-.181	-.166	-.178	-.155	-.115	-.077

NACA

TABLE II.- PRESSURE COEFFICIENT DATA FOR TWO OBLIQUE STATIONS - Concluded

(b) Station B

Orifice station (percent c)	Pressure coefficient								
	$\alpha = -2^{\circ}$	$\alpha = 0^{\circ}$	$\alpha = 1^{\circ}$	$\alpha = 3^{\circ}$	$\alpha = 5^{\circ}$	$\alpha = 7^{\circ}$	$\alpha = 9^{\circ}$	$\alpha = 11^{\circ}$	$\alpha = 13^{\circ}$
Upper surface									
12.077	0.268	0.185	0.139	0.085	-0.178	-0.280	-0.376	-0.460	-0.524
23.188	.131	.062	.027	-.041	-.176	-.280	-.360	-.432	-.488
36.473	.027	-.037	-.069	-.133	-.176	-.306	-.378	-.438	-.488
47.101	-.049	-.107	-.138	-.193	-.232	-.336	-.404	-.456	-.498
63.043	-.142	-.192	-.220	-.264	-.306	-.371	-.430	-.448	
73.671	-.204	-.252	-.268	-.320	-.358	-.391	-.420	-.444	-.472
82.609	-.256	-.250	-.234	-.362	-.400	-.377	-.412	-.442	-.470
94.203	-.264	-.218	-.218	-.334	-.346	-.344	-.384	-.420	-.450
Lower surface									
2.174	0.093	0.307	0.381	0.488	0.563	0.623	0.678	0.725	0.762
8.937	.087	.200	.245	.325	.393	.457	.518	.579	.633
17.633	.021	.109	.143	.212	.278	.339	.402	.464	.517
29.710	-.062	.006	.035	.097	.158	.218	.280	.340	.397
42.512	-.147	-.088	-.062	-.008	.055	.110	.171	.229	.284
56.522	-.222	-.169	-.146	-.091	-.035	.018	.075	.128	.181
68.599	-.284	-.233	-.213	-.162	-.111	-.062	-.010	.042	.092
80.193	-.259	-.249	-.263	-.217	-.171	-.125	-.074	-.027	.021
93.961	-.249	-.218	-.226	-.266	-.237	-.193	-.147	-.104	-.058

NACA

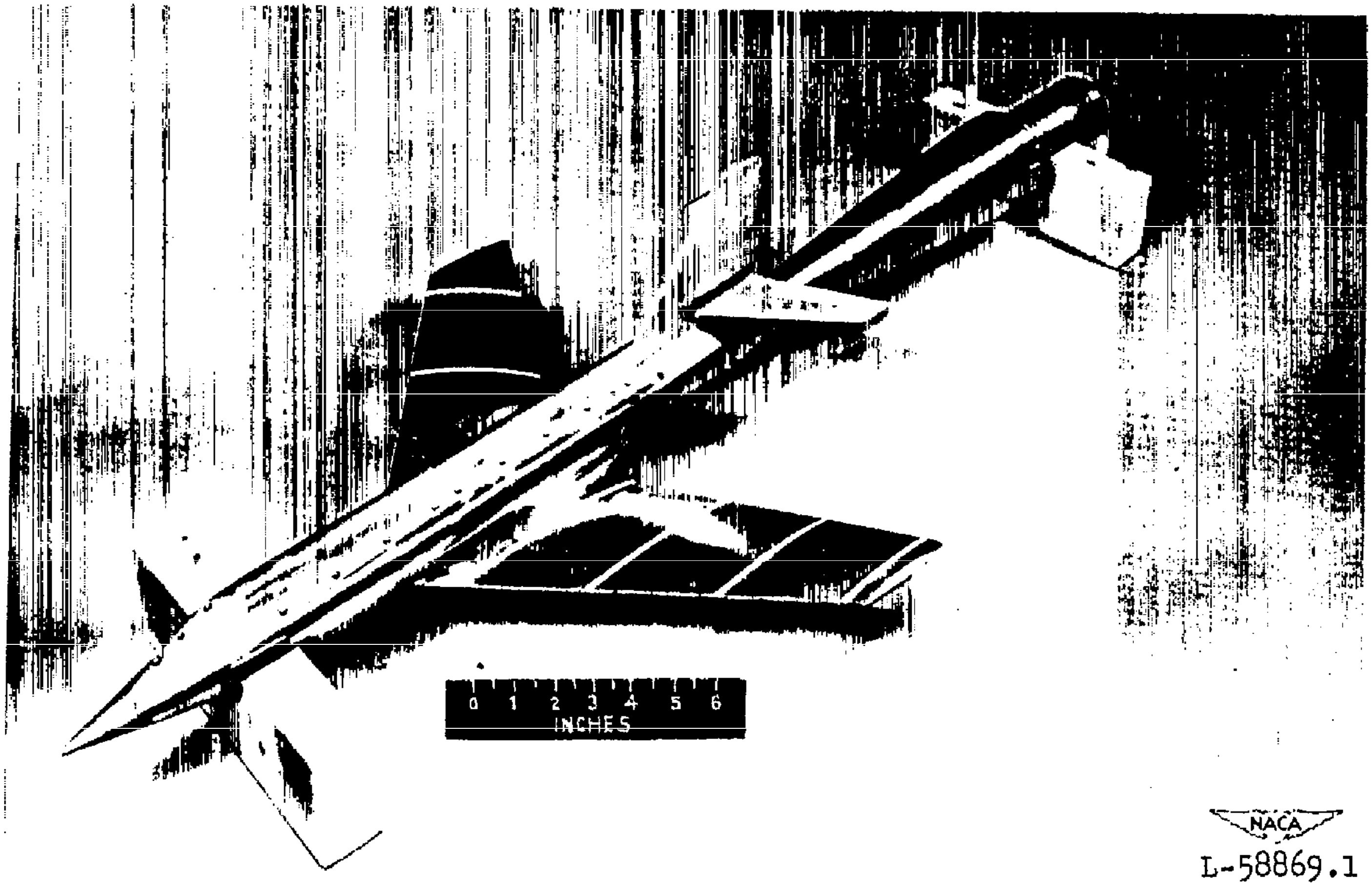

Figure 1.- Pressure model of the supersonic aircraft configuration tested in the Langley 4- by 4-foot supersonic tunnel.

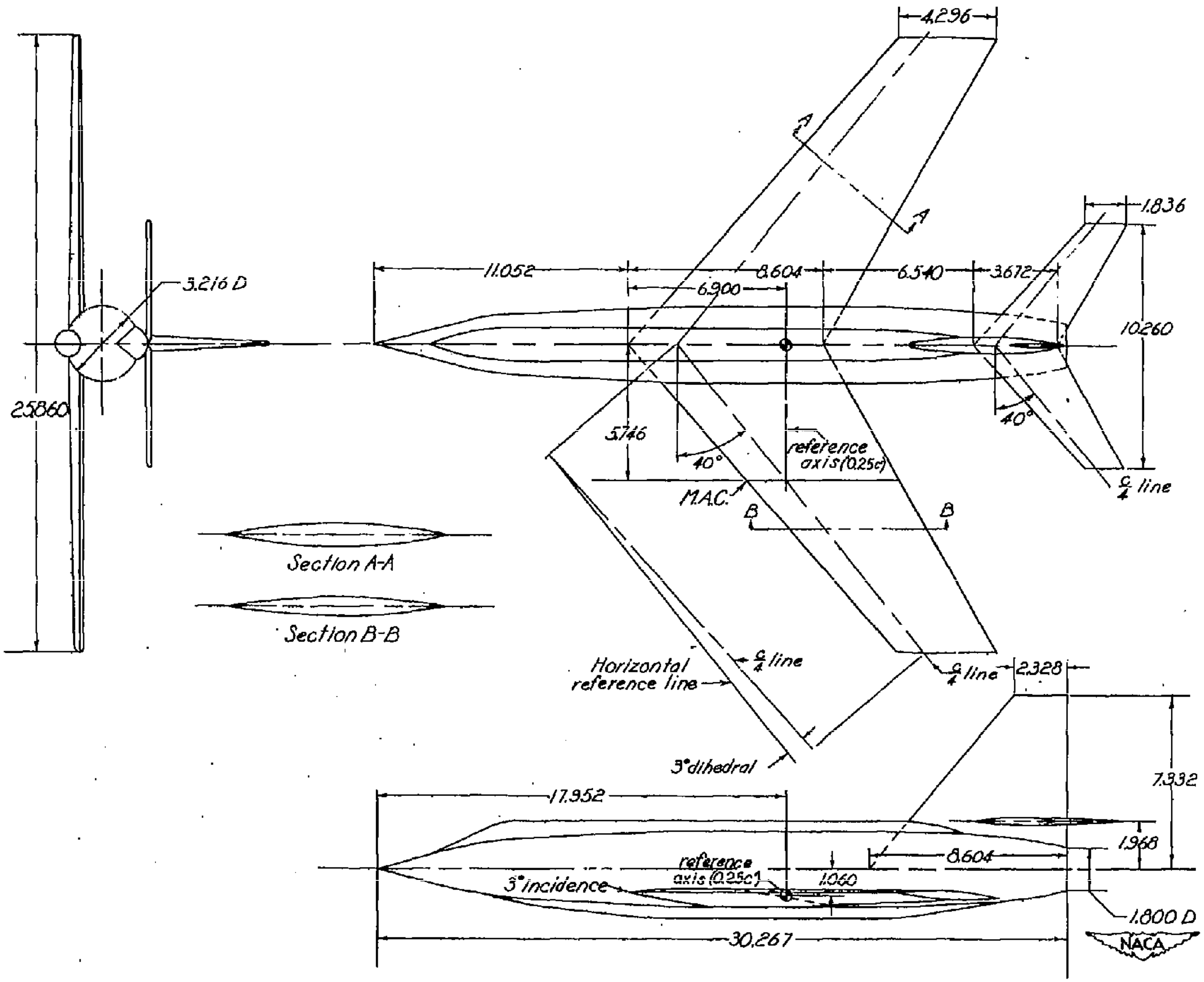

Figure 2.-- Details of model of supersonic aircraft configuration. (Dimensions are in inches unless otherwise noted.)

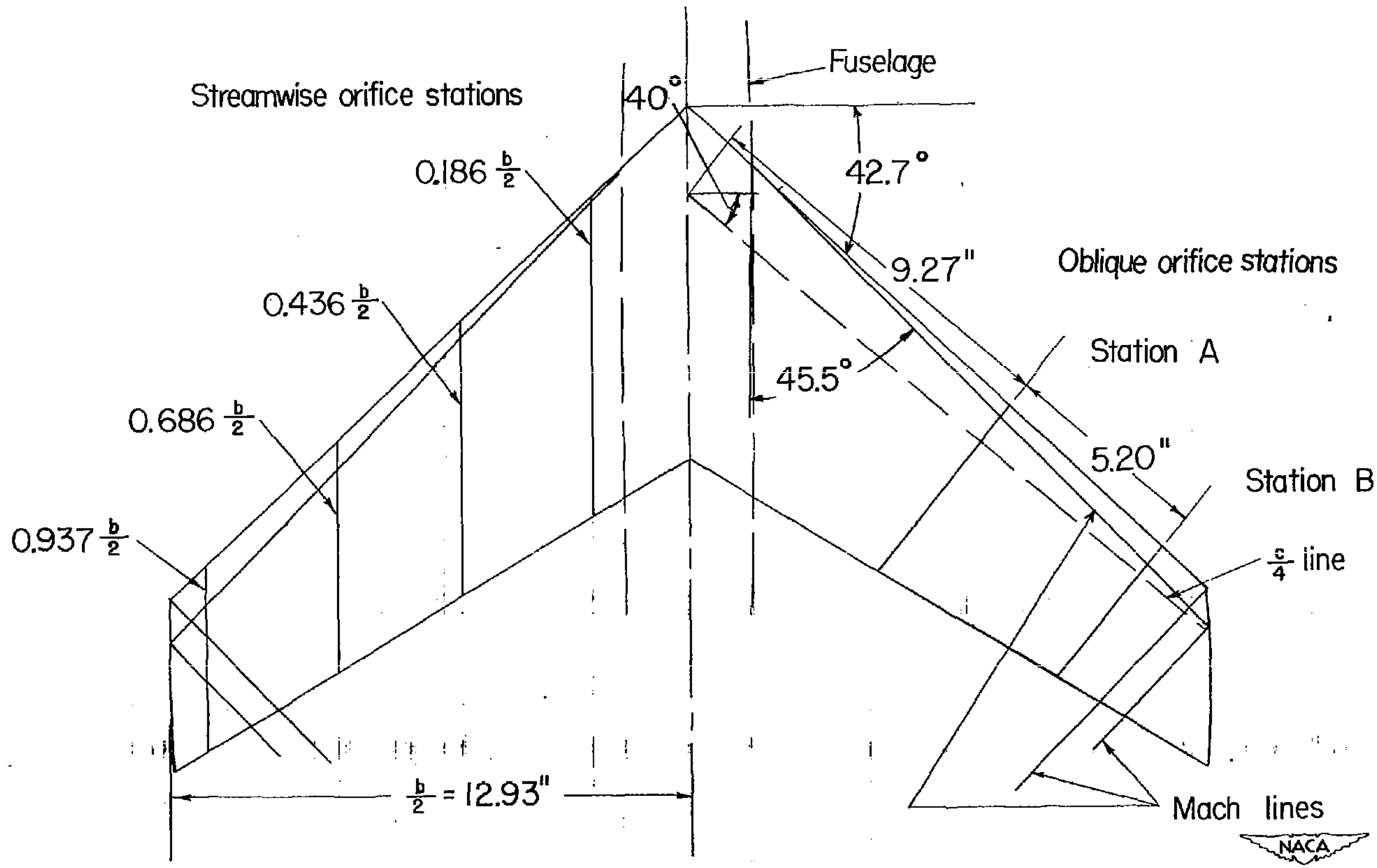

Figure 3.- Schematic view of wing showing orifice stations and Mach lines.

Figure 4.- Downstream view of test model mounted in the Langley 4- by 4-foot supersonic tunnel.

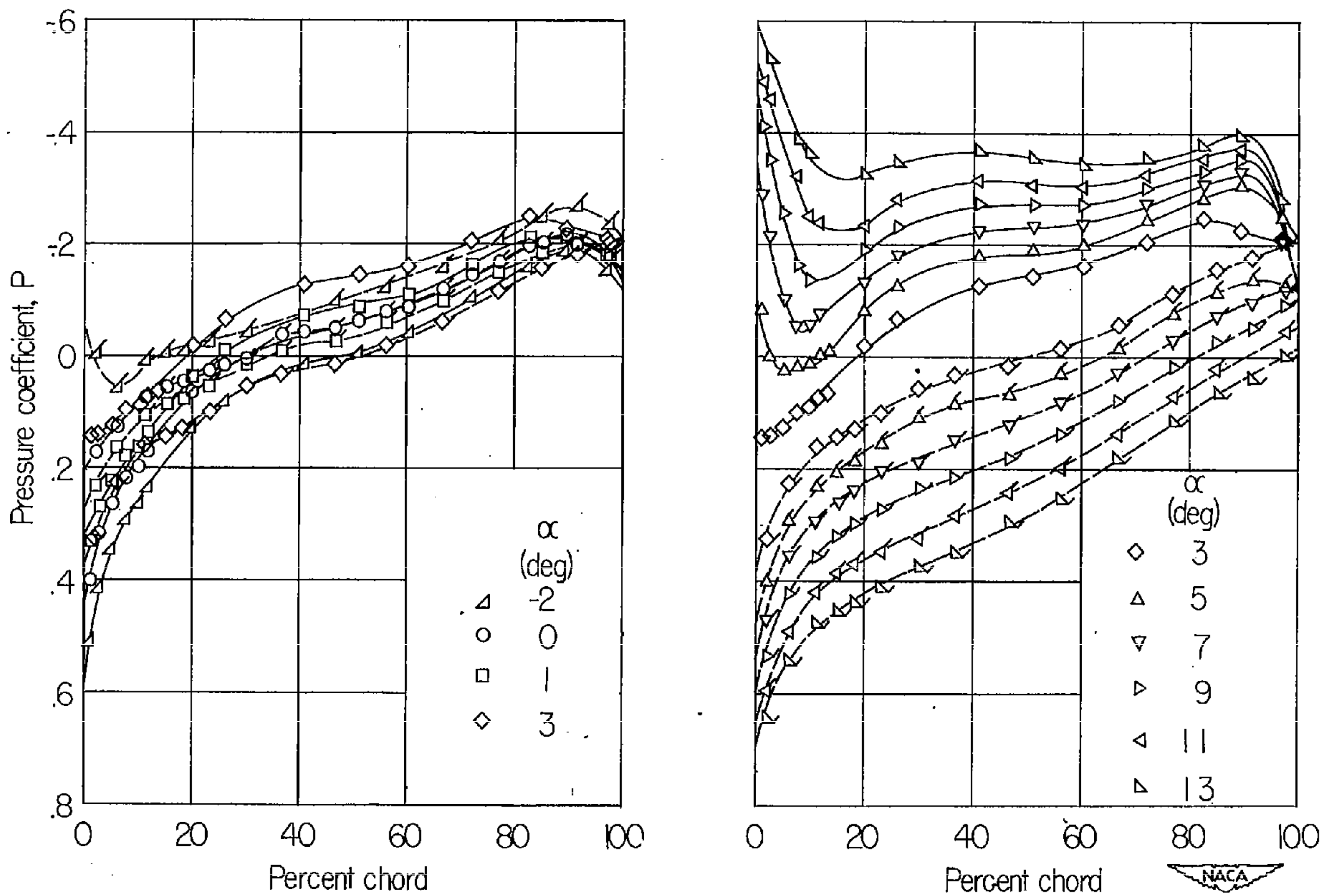

(a) $y/\frac{b}{2} = 0.186$.

Figure 5.- Variation of pressure distribution with angle of attack at four streamwise stations. Flagged symbols denote lower surface. M = 1.40.

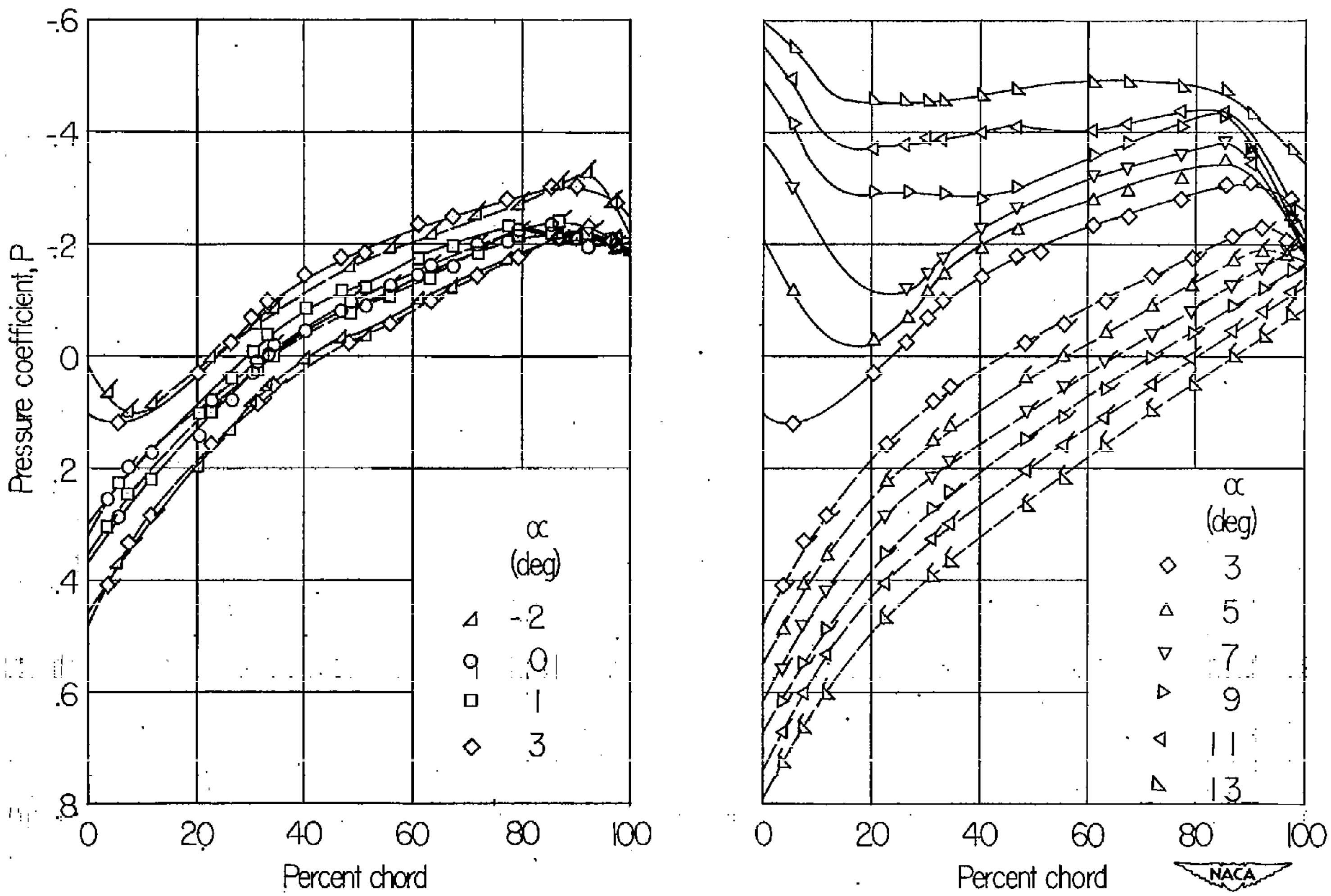

(b) $y/\frac{b}{2}$ = 0.436.

Figure 5.- Continued.

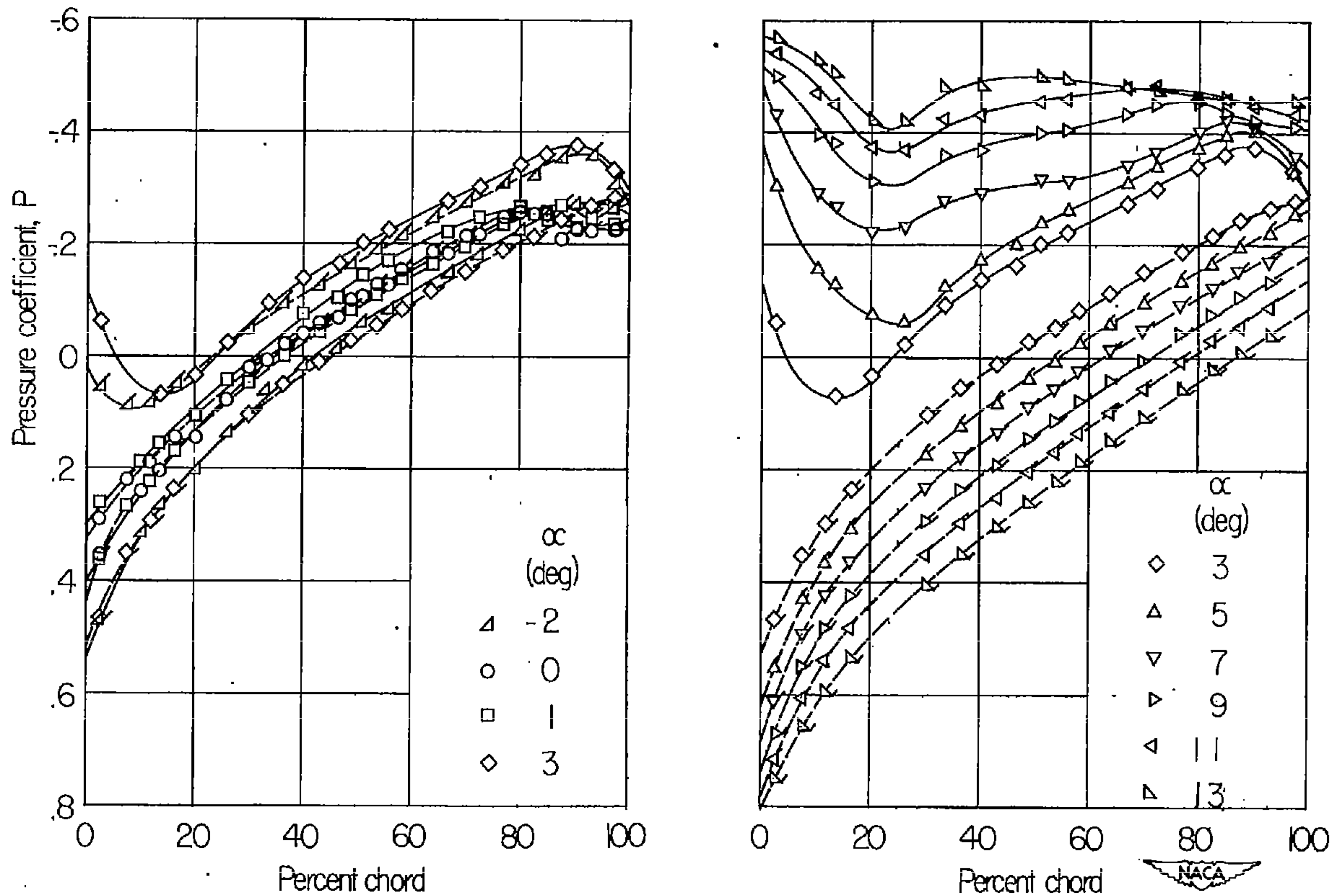

(c) $y/\frac{b}{2} = 0.686$.

Figure 5.- Continued.

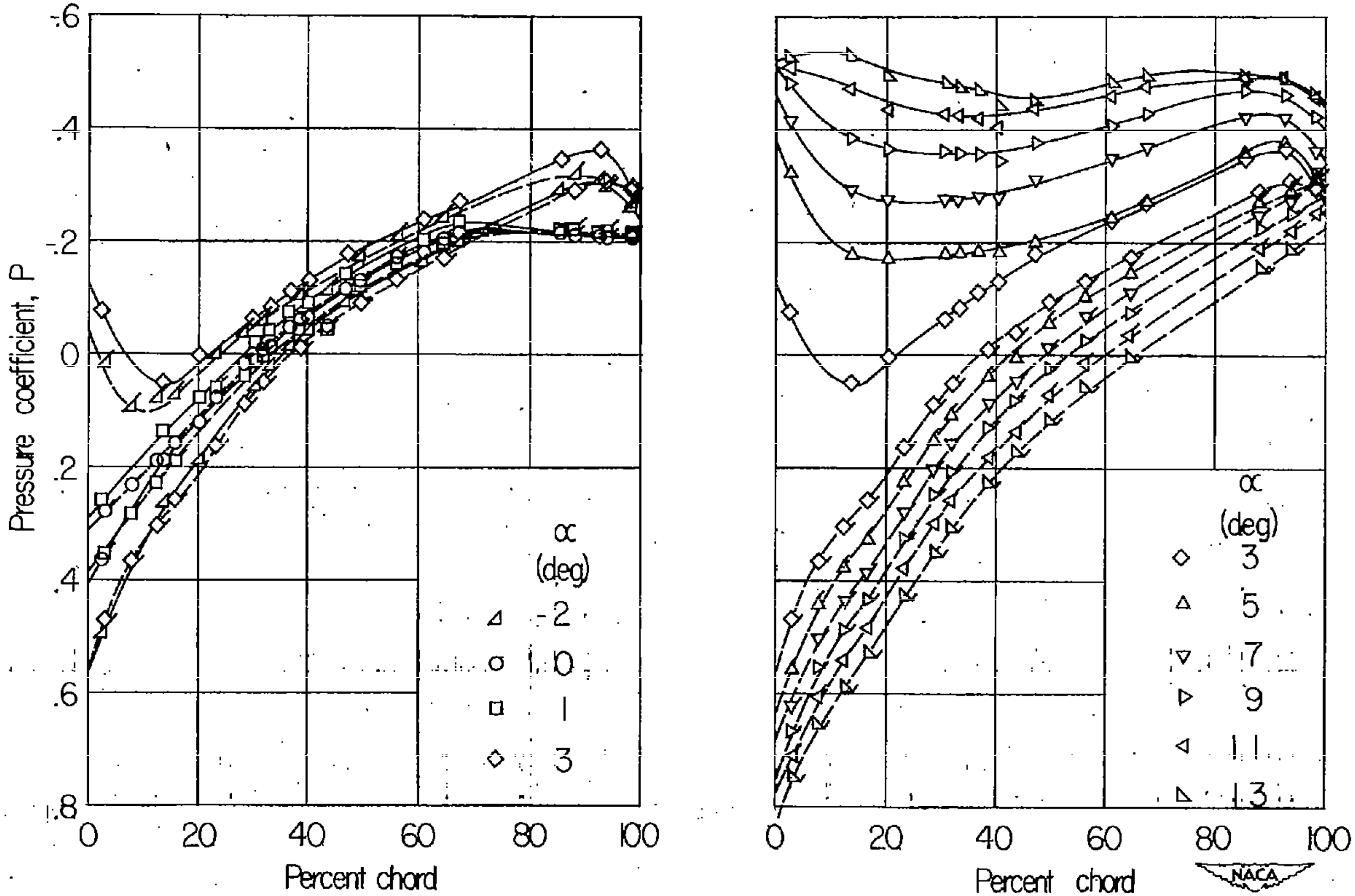

(d) $y/\frac{b}{2} = 0.937$

Figure 5.- Concluded.

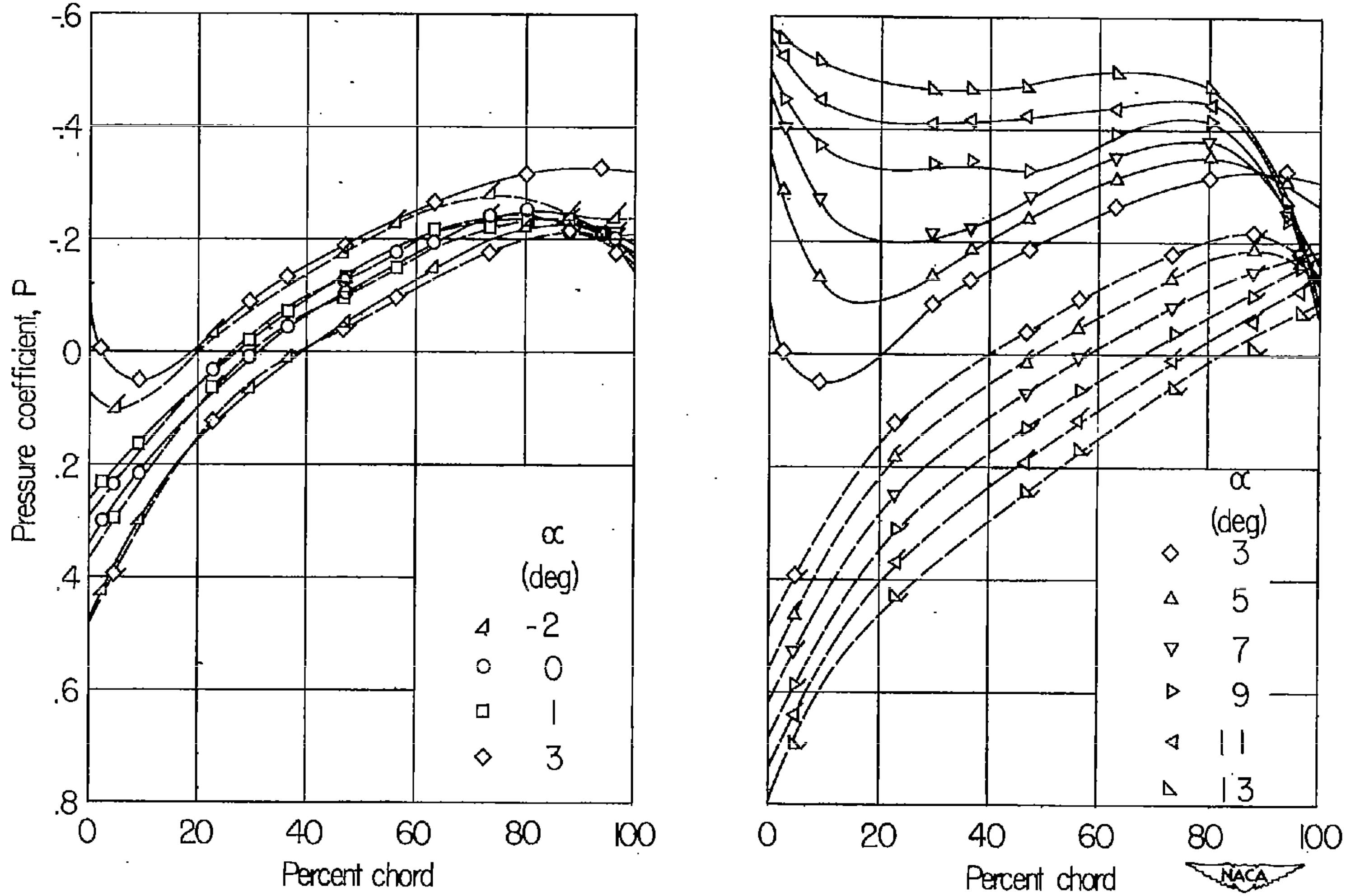

(a) Station A.

Figure 6.- Variation of pressure distribution with angle of attack at two oblique stations. Flagged symbols denote lower surface. M = 1.40.

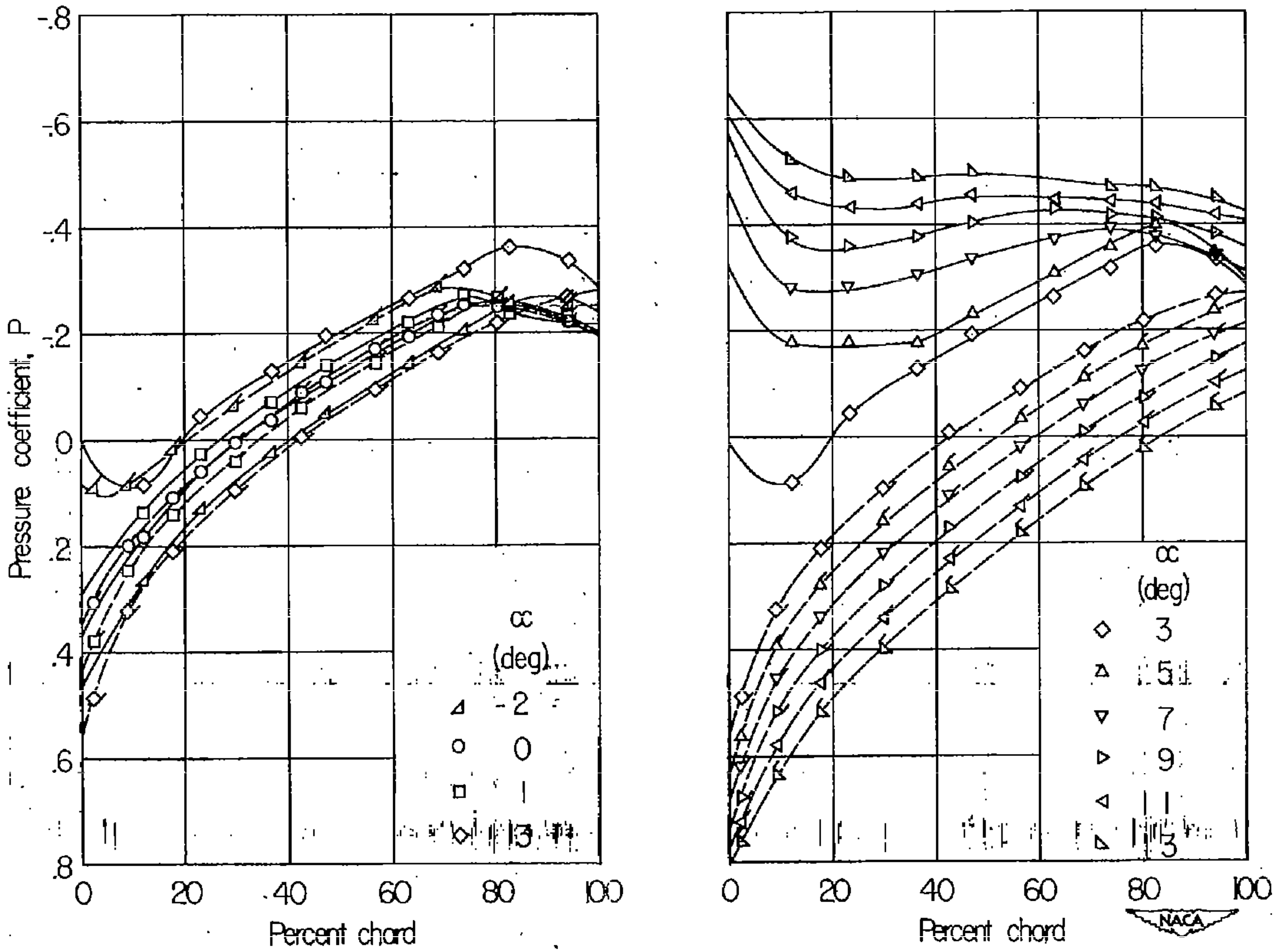

(b) Station B.

Figure 6.- Concluded.

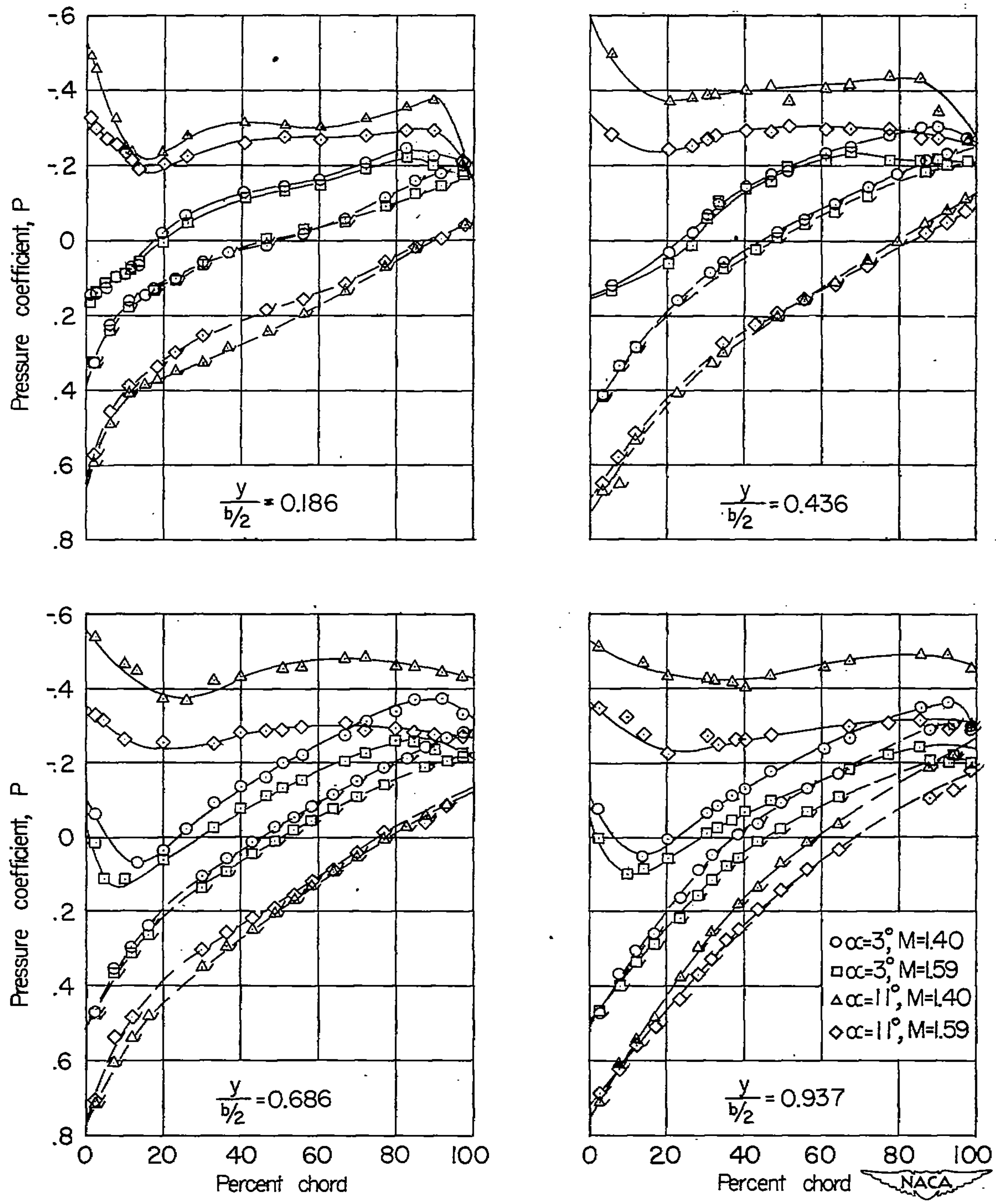

Figure 7.- Comparison of pressure distribution at two Mach numbers.

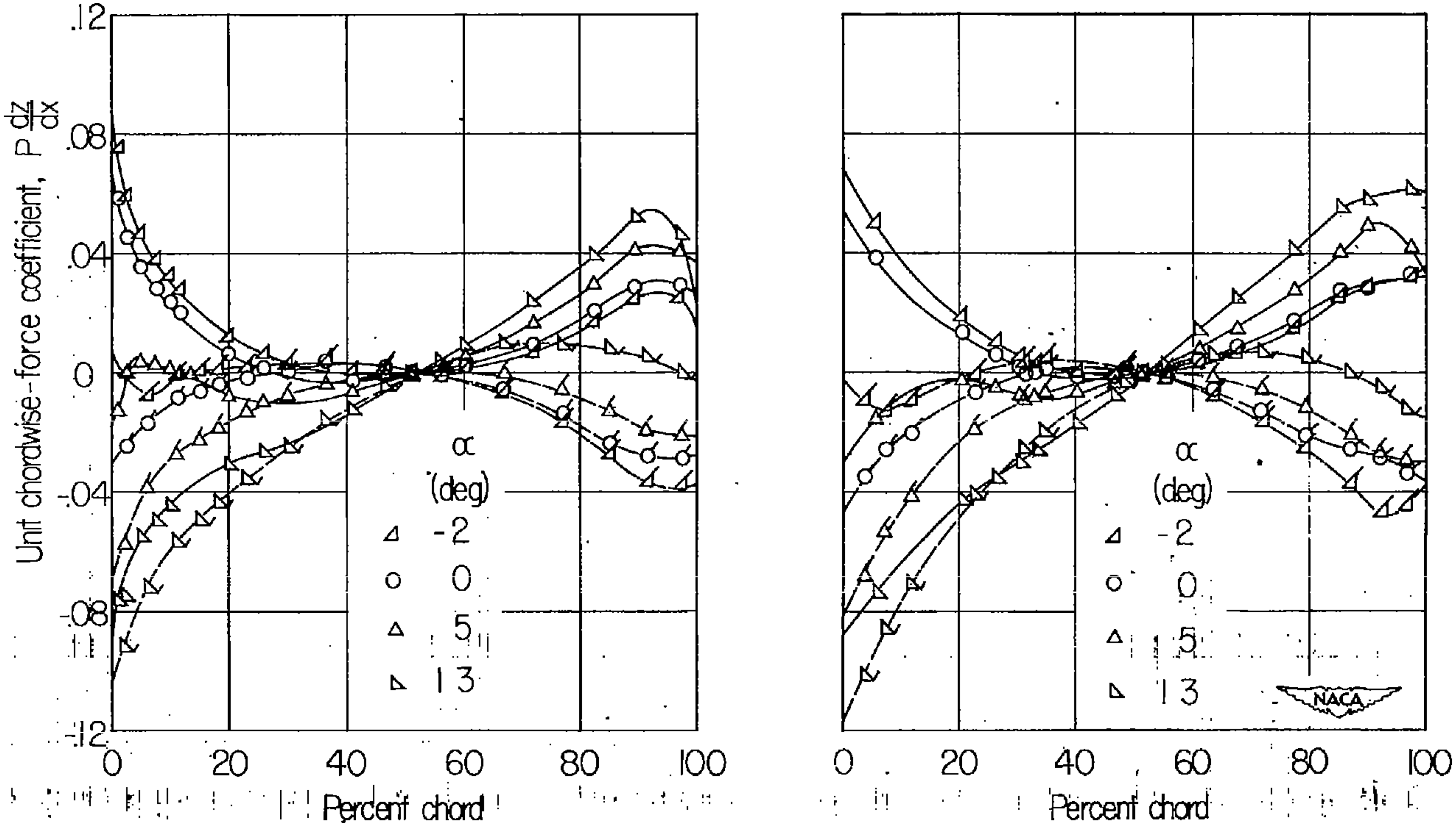

(a) $y/\frac{b}{2} = 0.186$.

(b) $y/\frac{b}{2} = 0.436$.

Figure 8.- Variation of unit chordwise-force coefficient with angle of attack at four streamwise stations. Flagged symbols denote lower surface. M = 1.40.

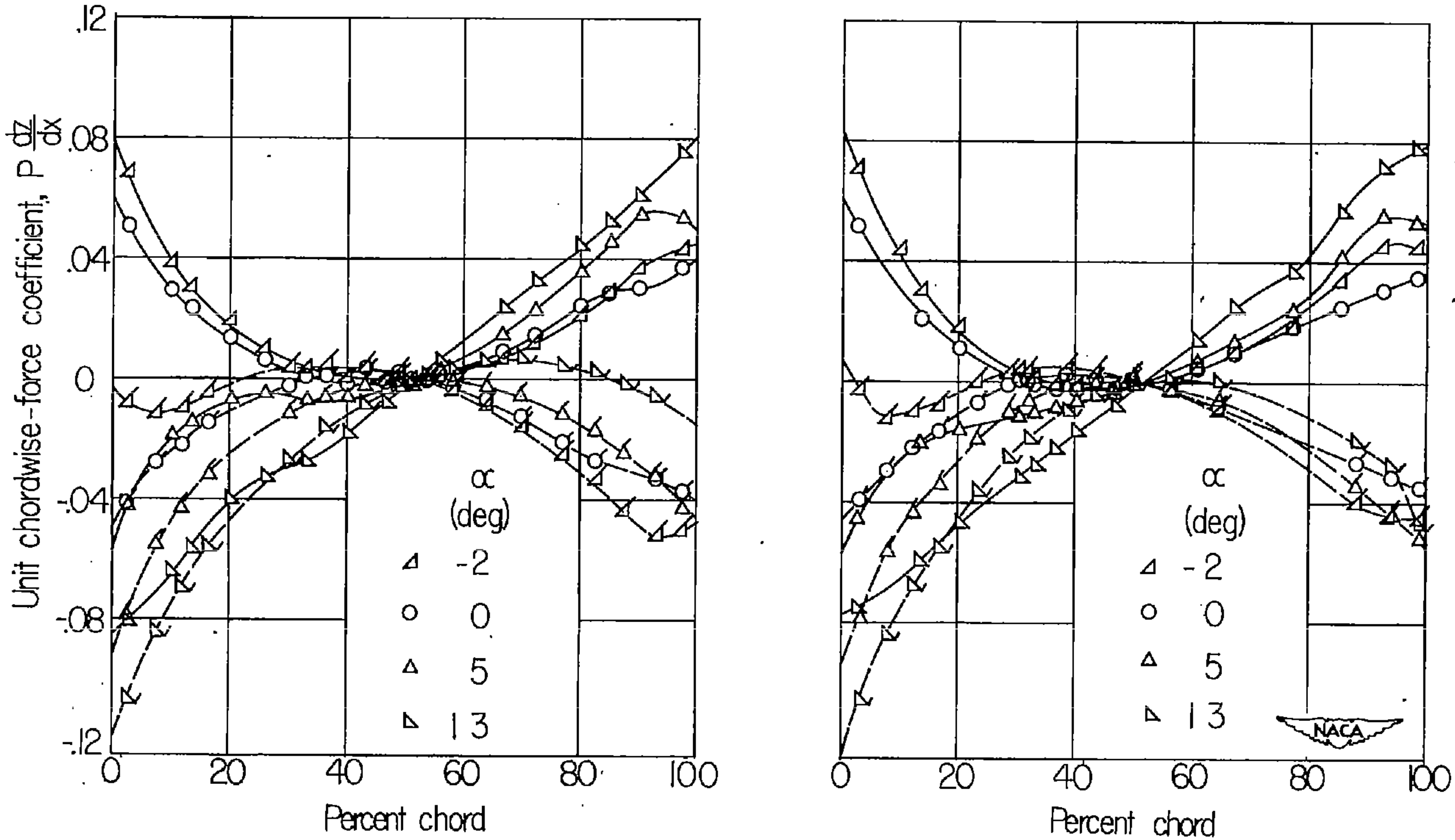

(c) $y/\frac{b}{2} = 0.686.$ (d) $y/\frac{b}{2} = 0.937.$

Figure 8.- Concluded.

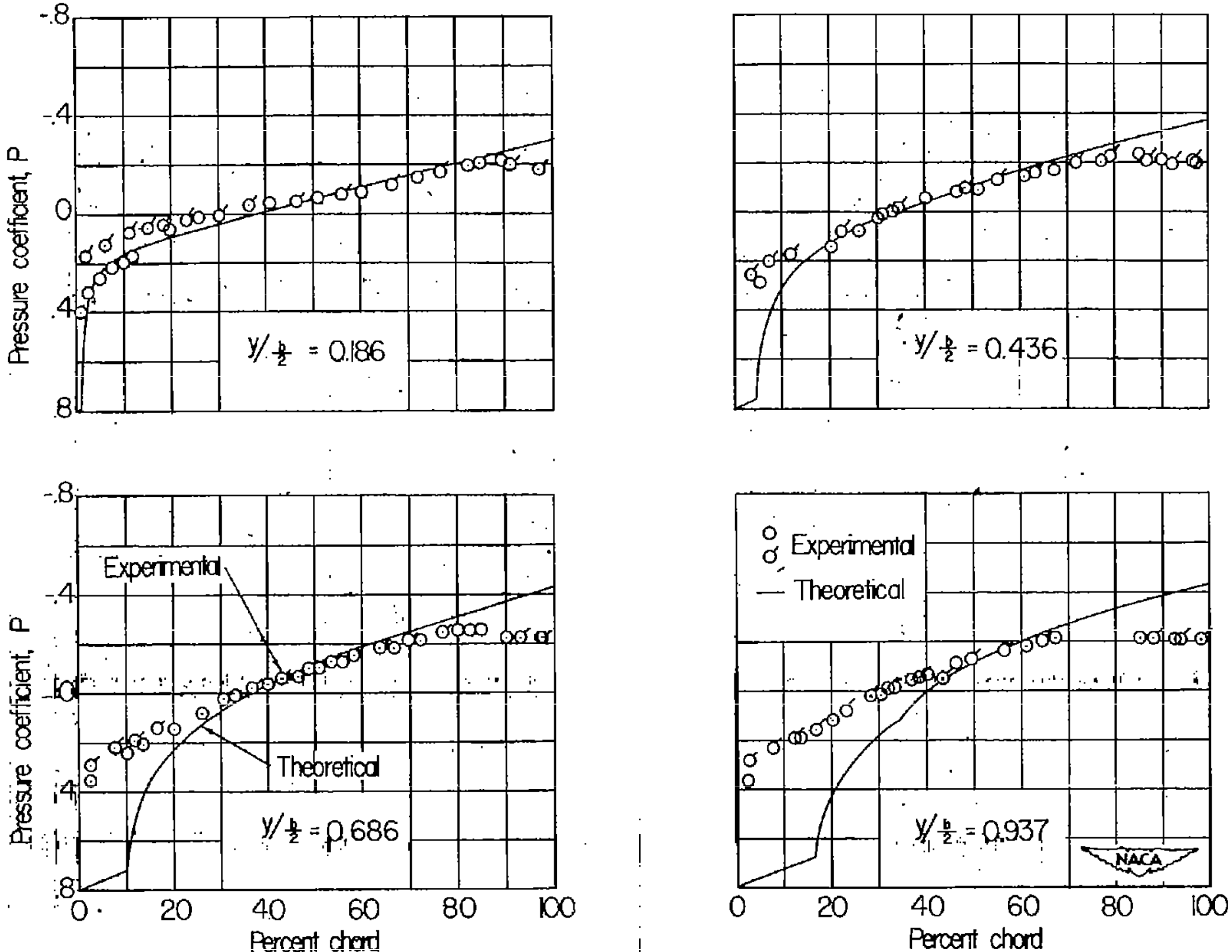

Figure 9.- Comparison of experimental and theoretical pressure distribution for zero angle of attack at four streamwise stations. Flagged symbols denote lower surface. M = 1.40.

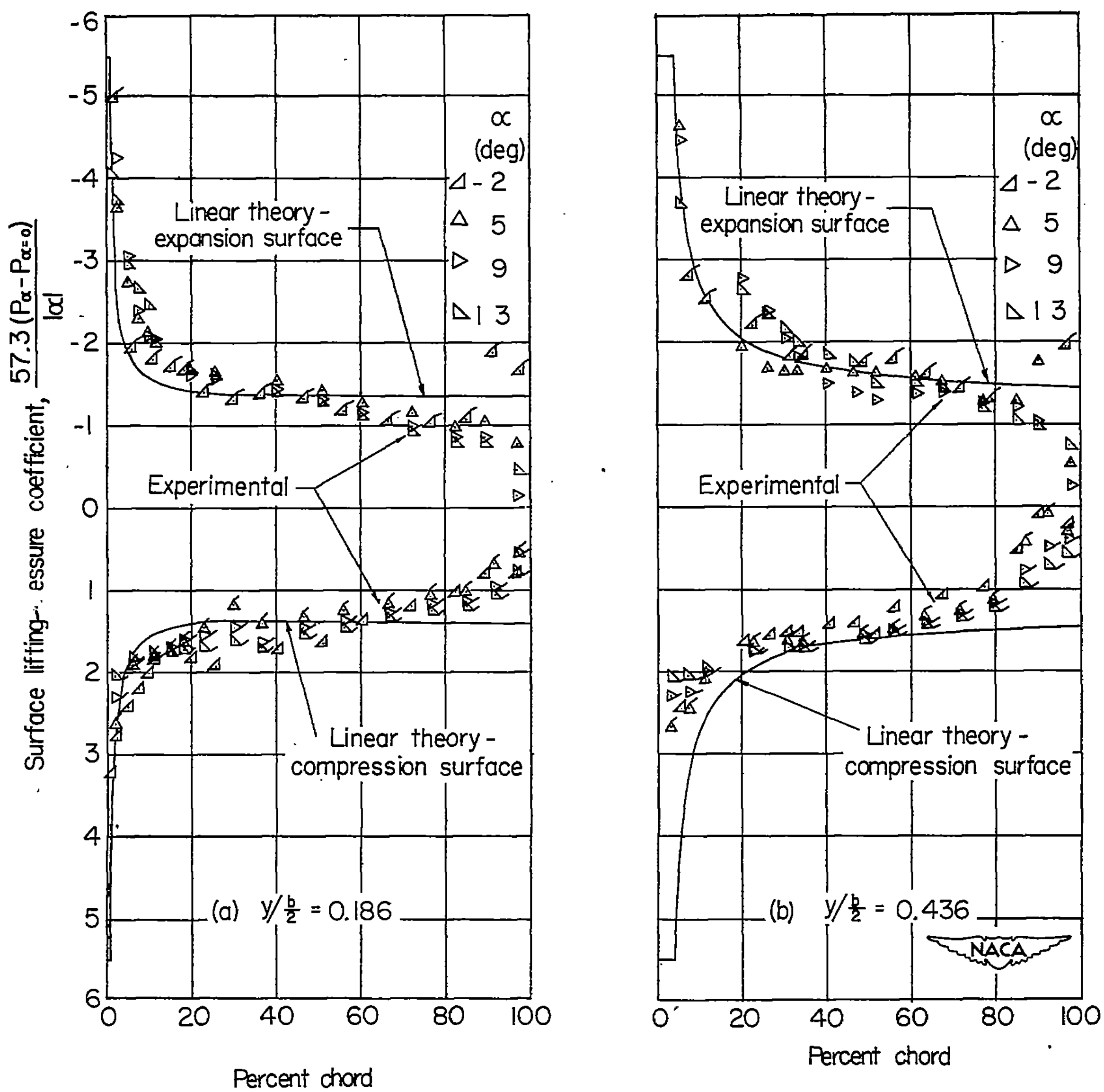

Figure 10.- Comparison of experimental and theoretical surface lifting-pressure coefficient for representative angles of attack at four streamwise stations. Flagged symbols denote lower surface. M = 1.40.

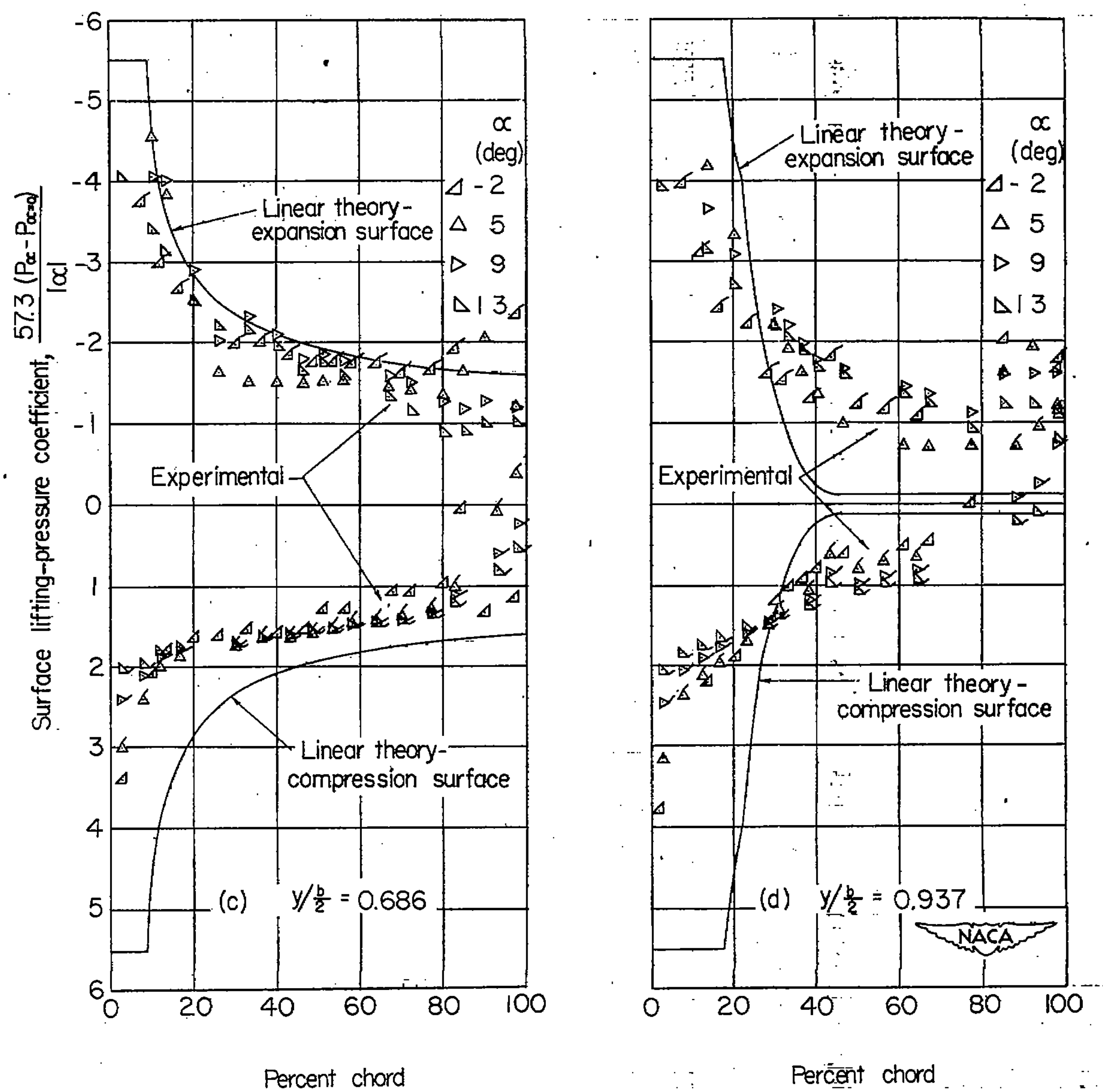

Figure 10.- Concluded.

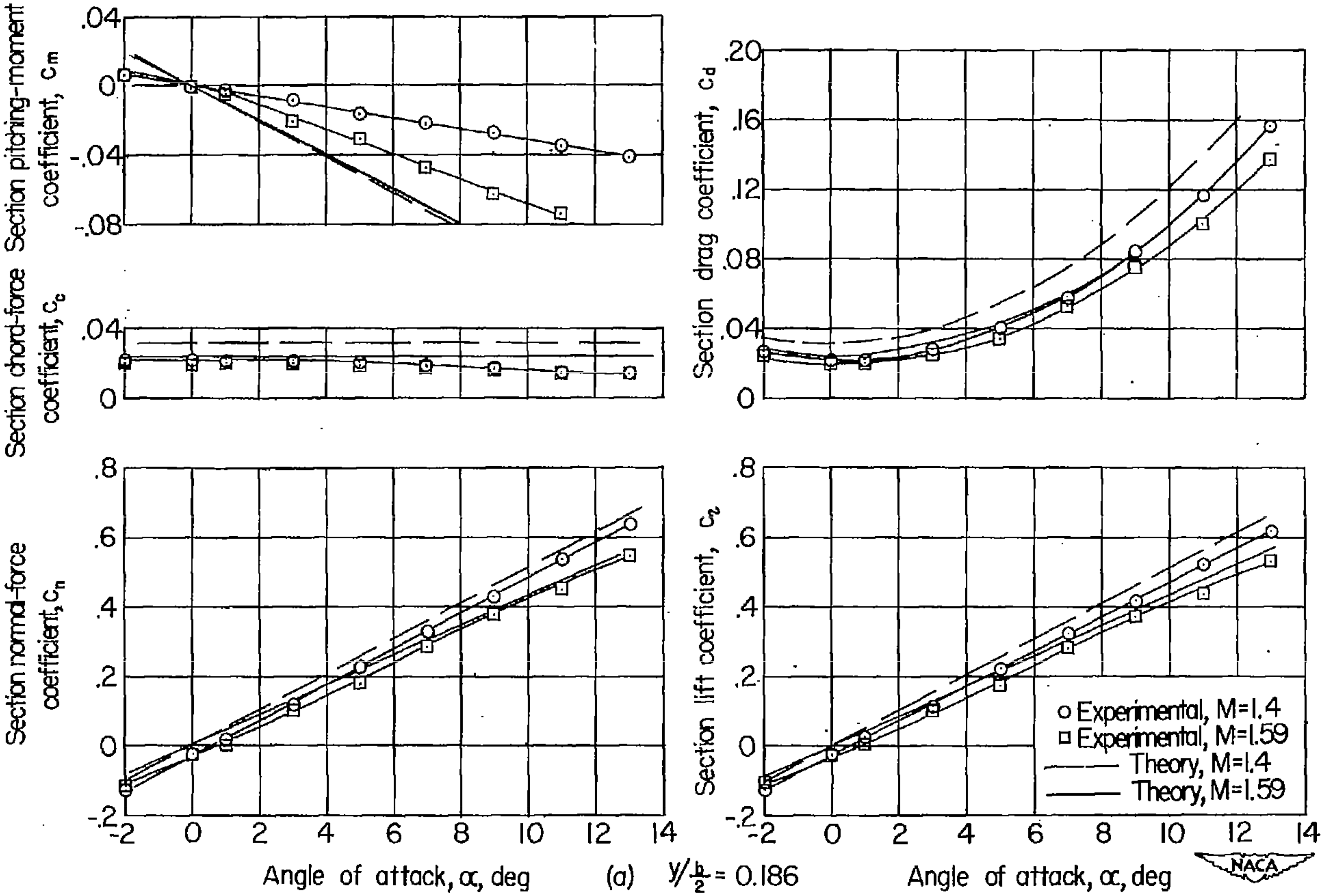

(a) $y/\frac{b}{2} = 0.186$

Figure 11.- Aerodynamic characteristics at four streamwise stations.

[redacted]

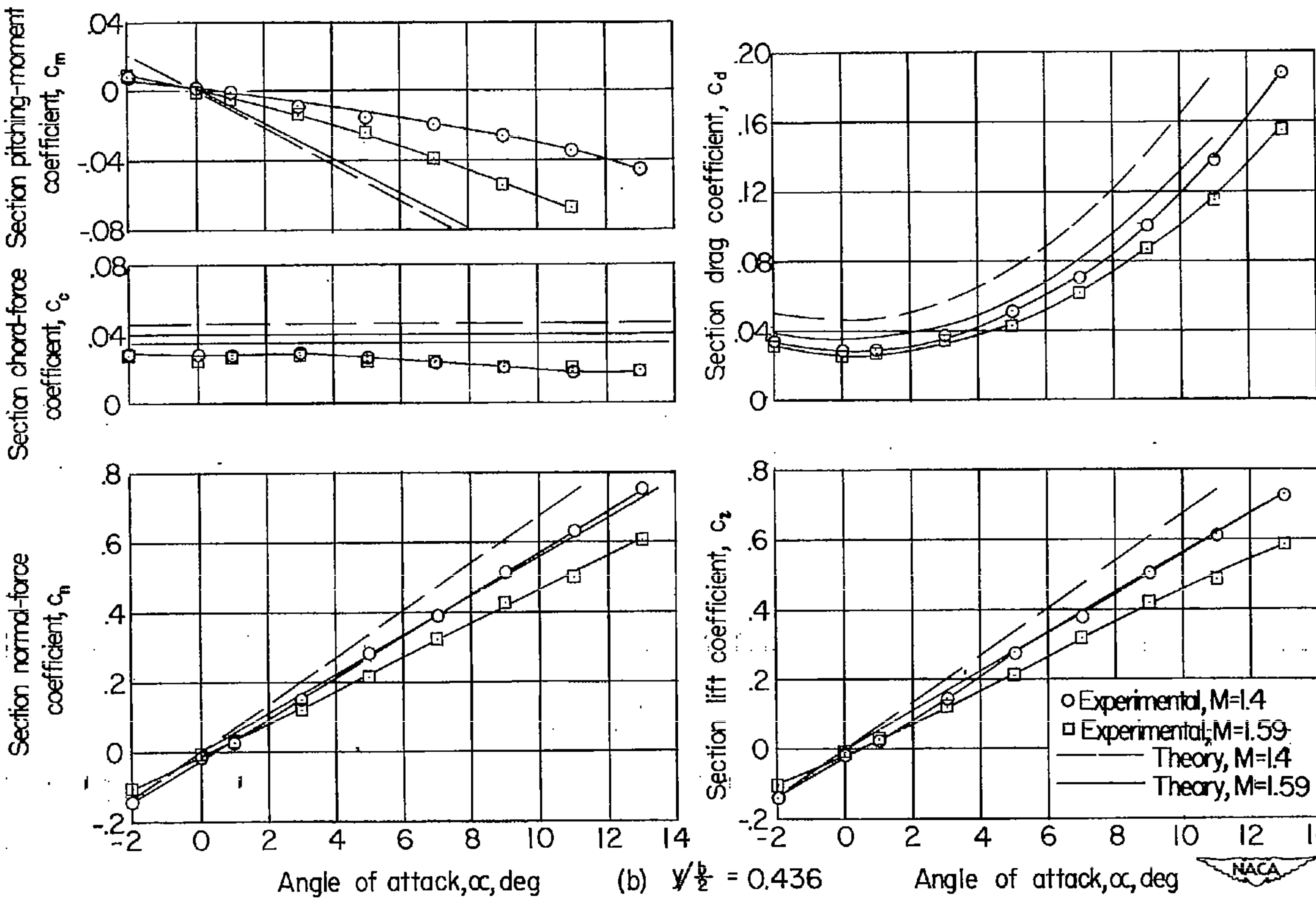

(b) $y/\frac{b}{2} = 0.436$

Figure 11.- Continued.

[redacted]

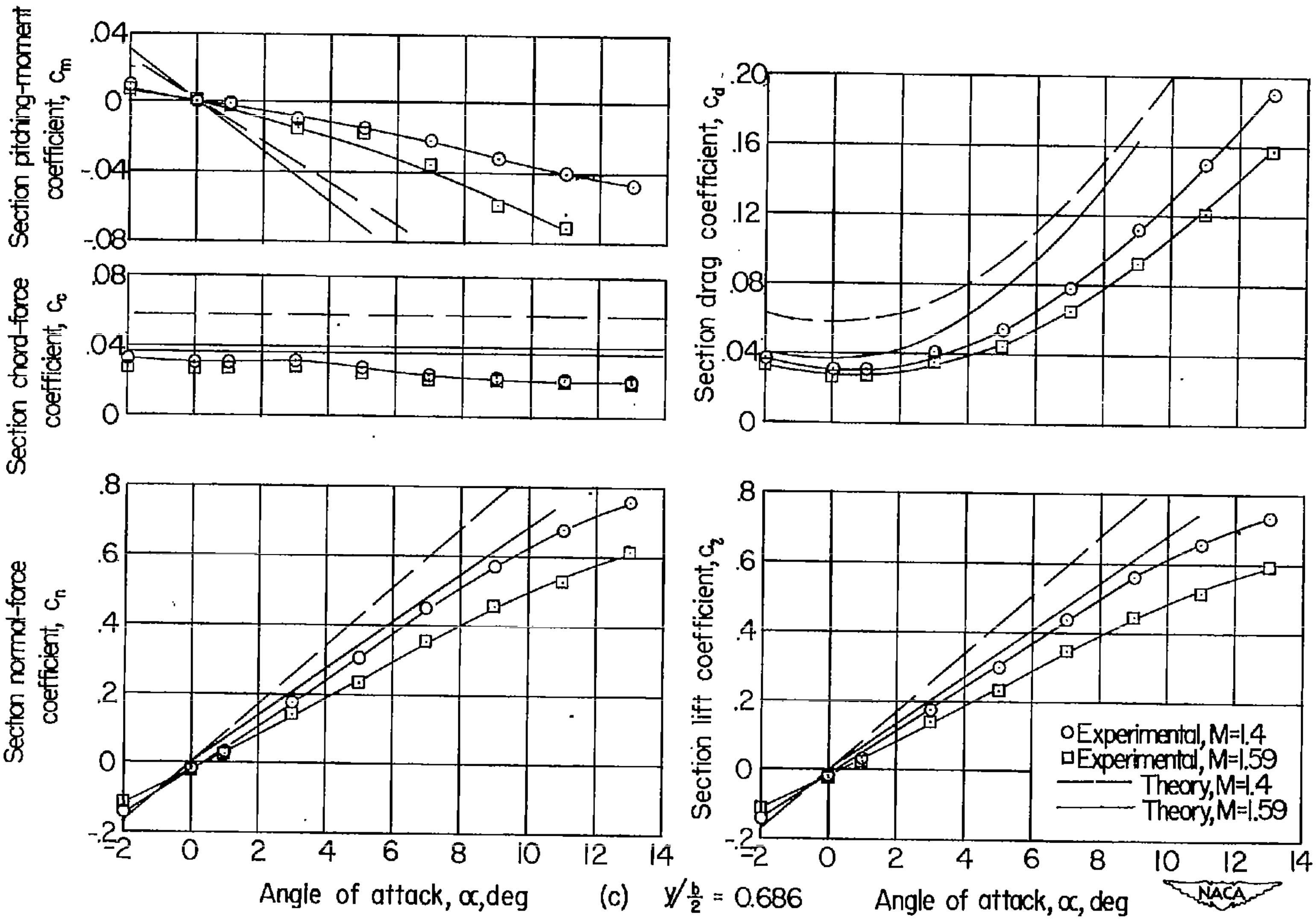

Figure 11.- Continued.

[redacted]

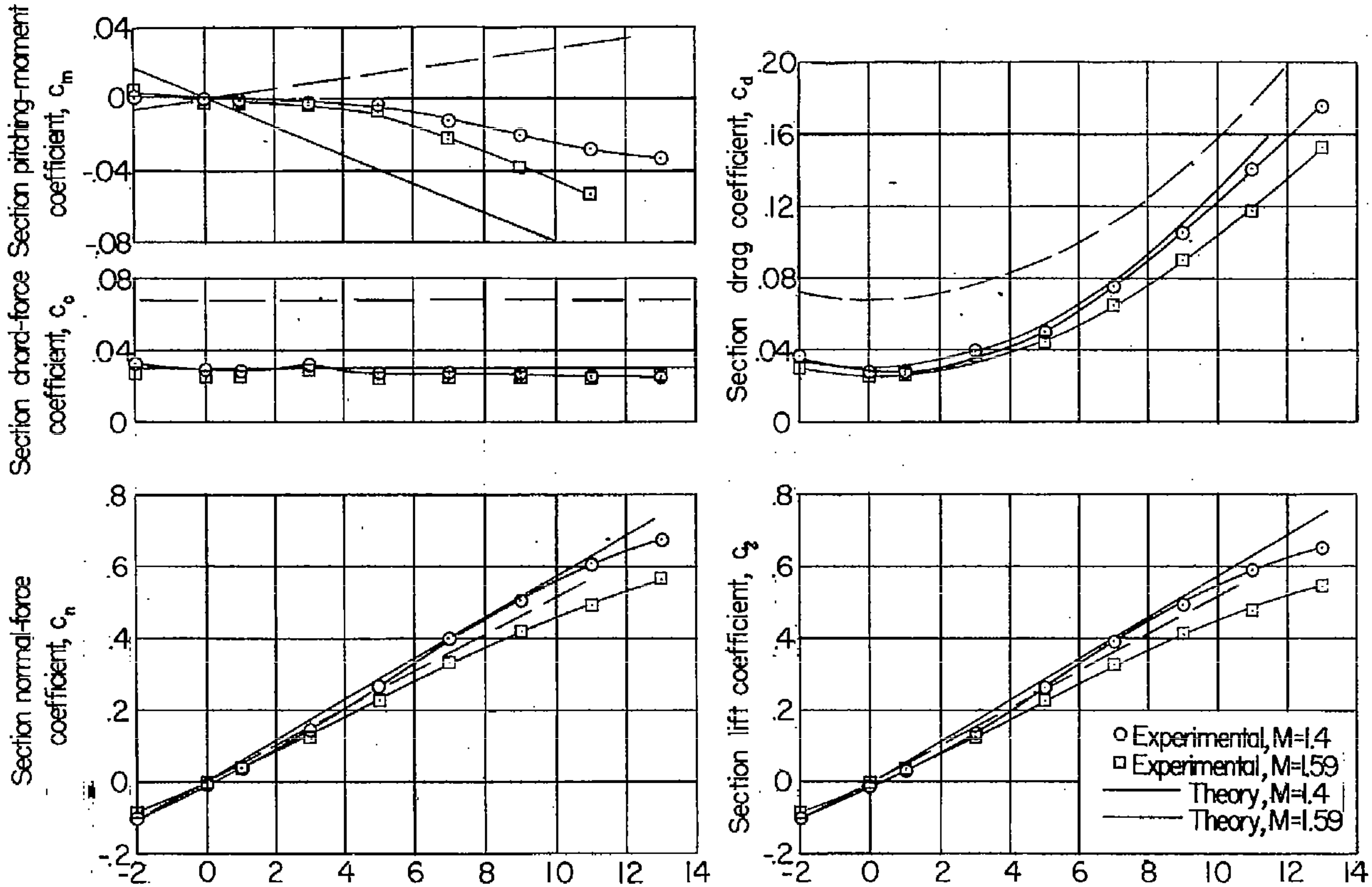

(d) $y/\frac{b}{2} = 0.937$

Figure 11.- Concluded.

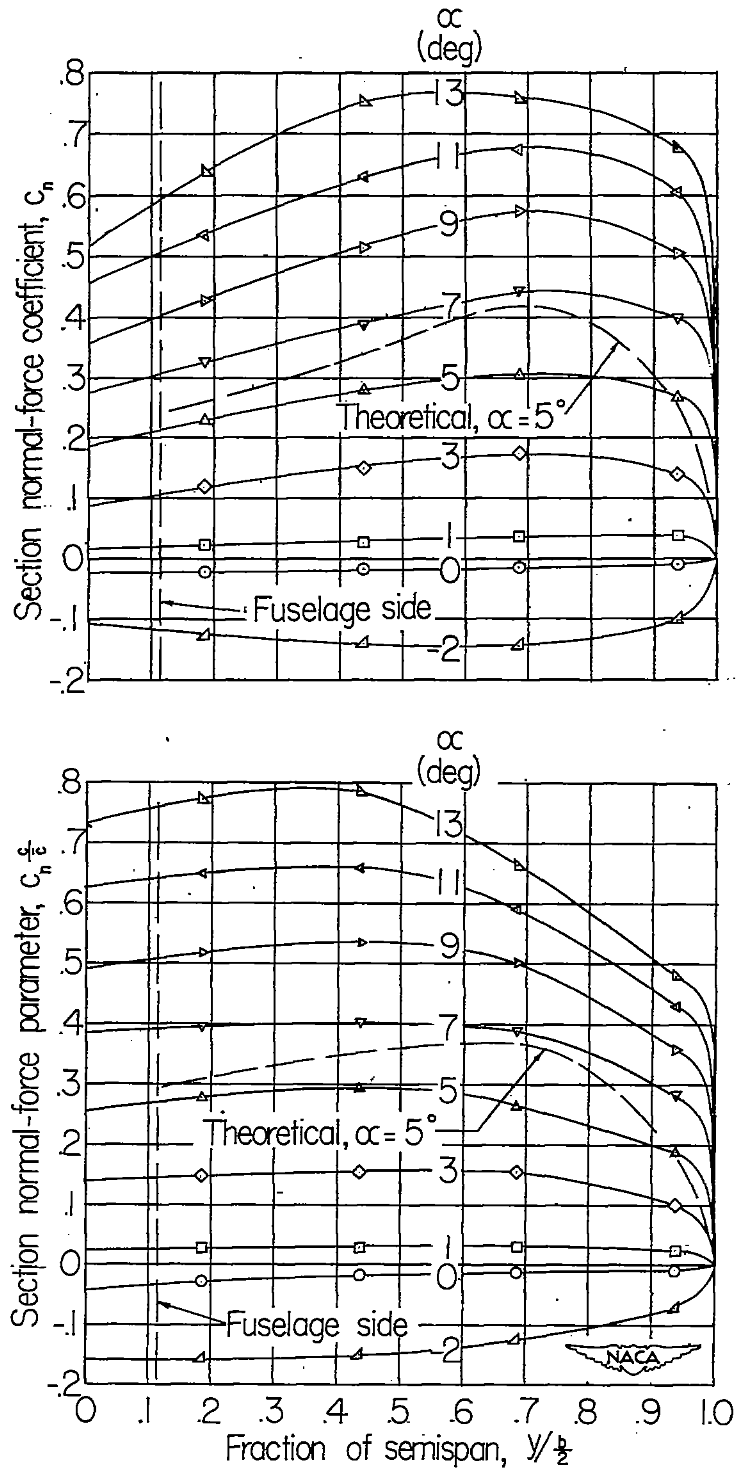

Figure 12.- Span-load distribution for representative angles of attack. M = 1.40.

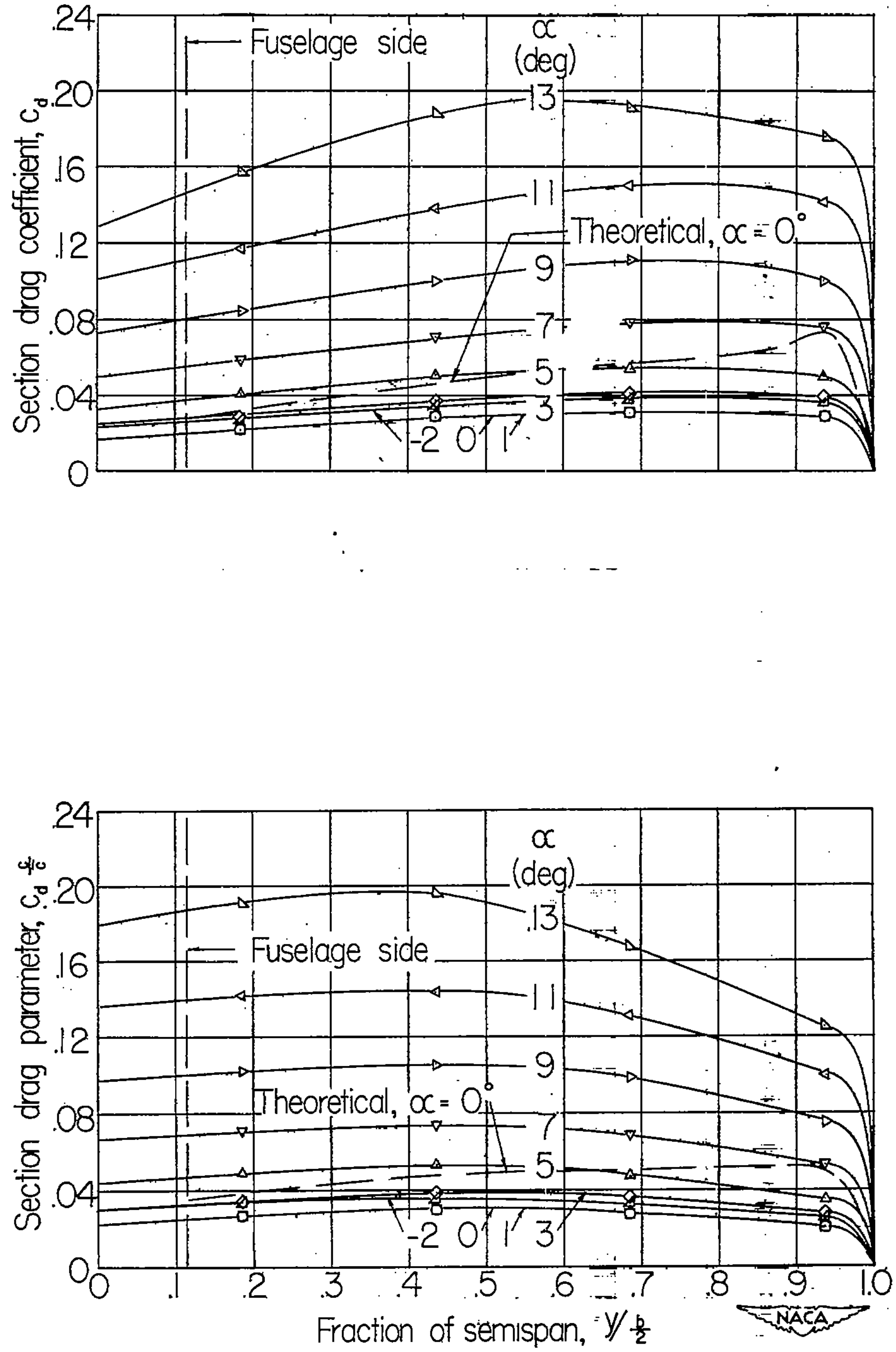

Figure 13.- Spanwise distribution of drag for representative angles of attack. M = 1.40.

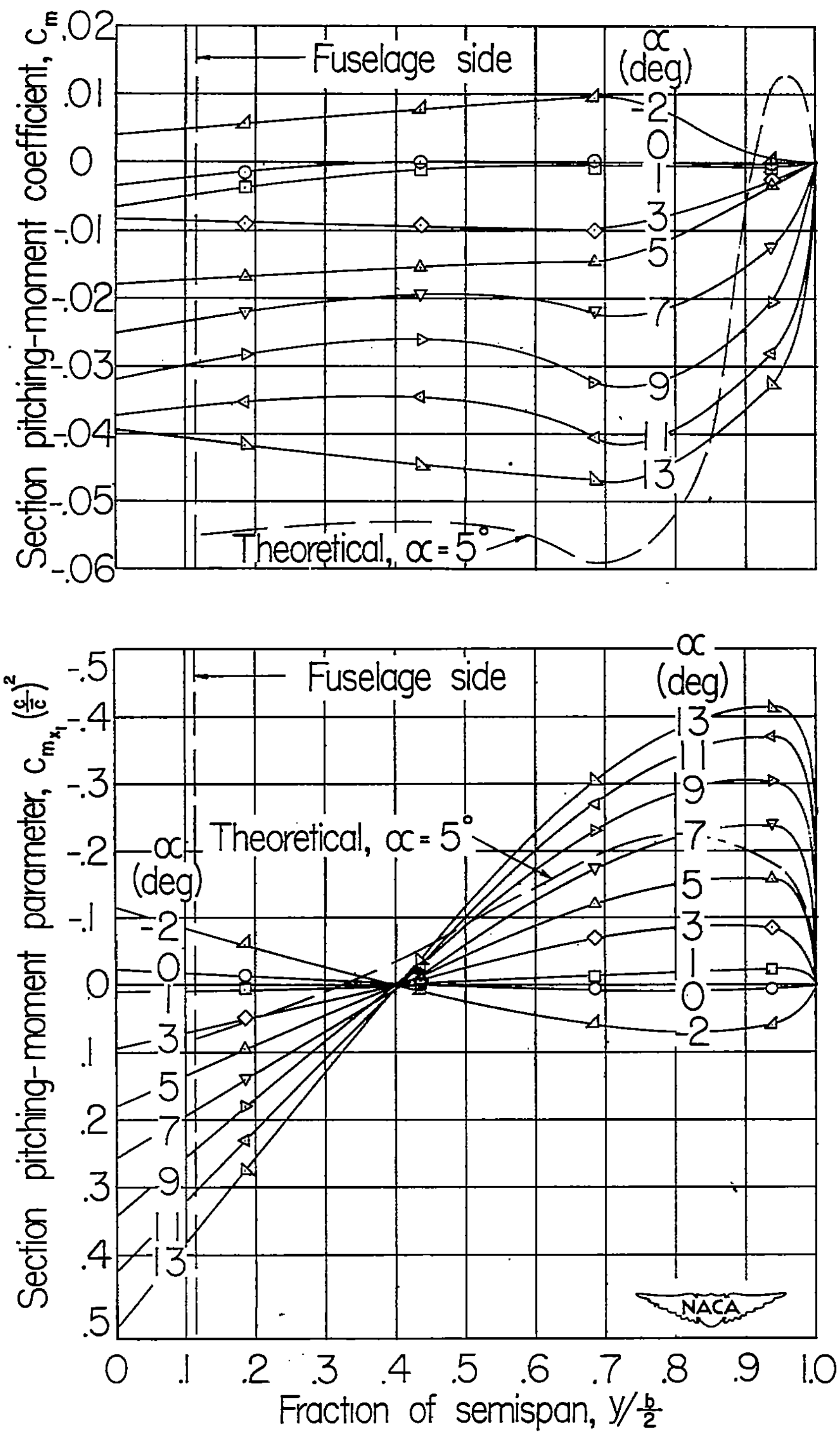

Figure 14.- Spanwise distribution of pitching moment for representative angles of attack. M = 1.40.

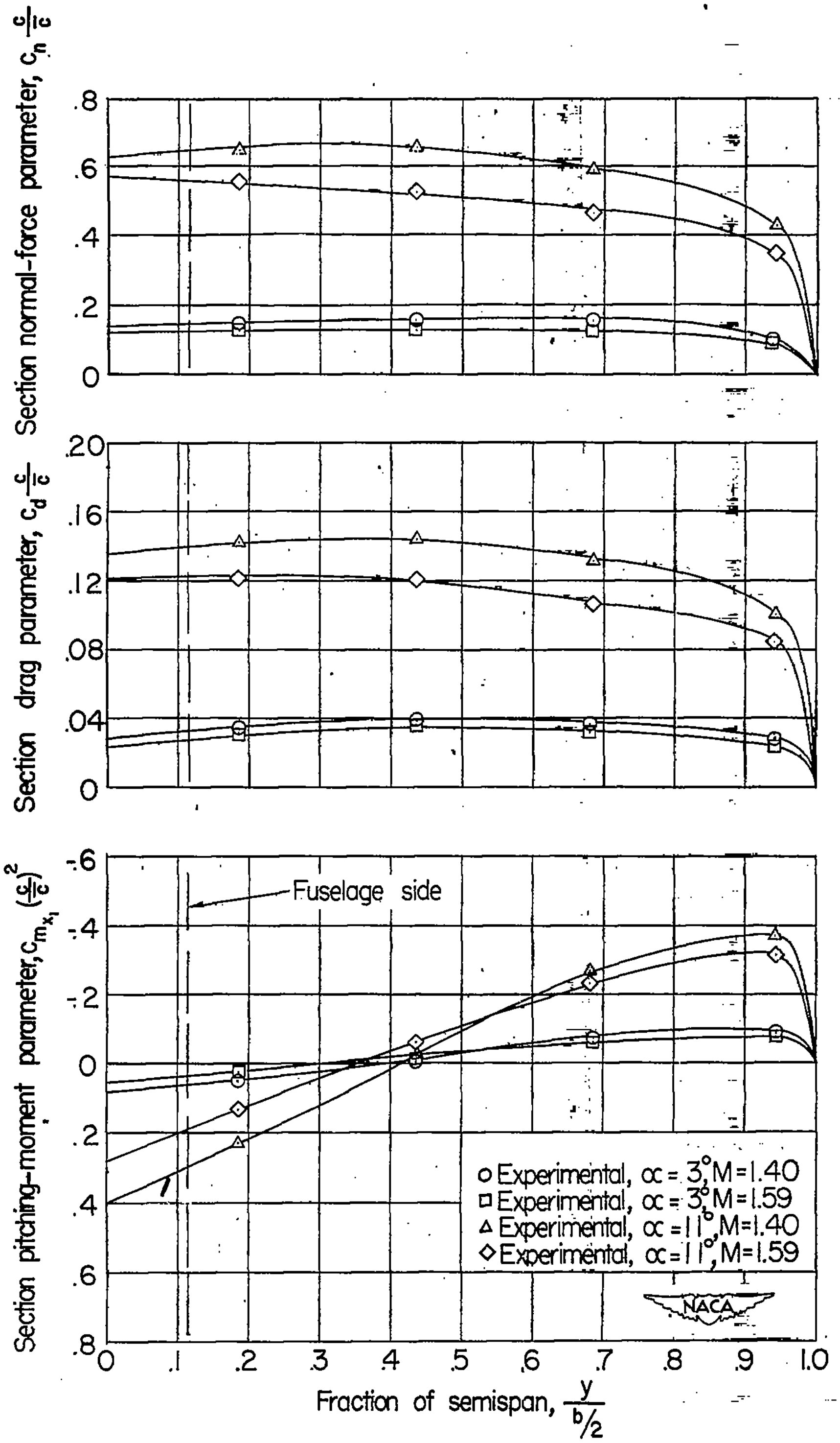

Figure 15.- Comparison of spanwise normal-force, drag, and pitching-moment distribution at two angles of attack and two Mach numbers.

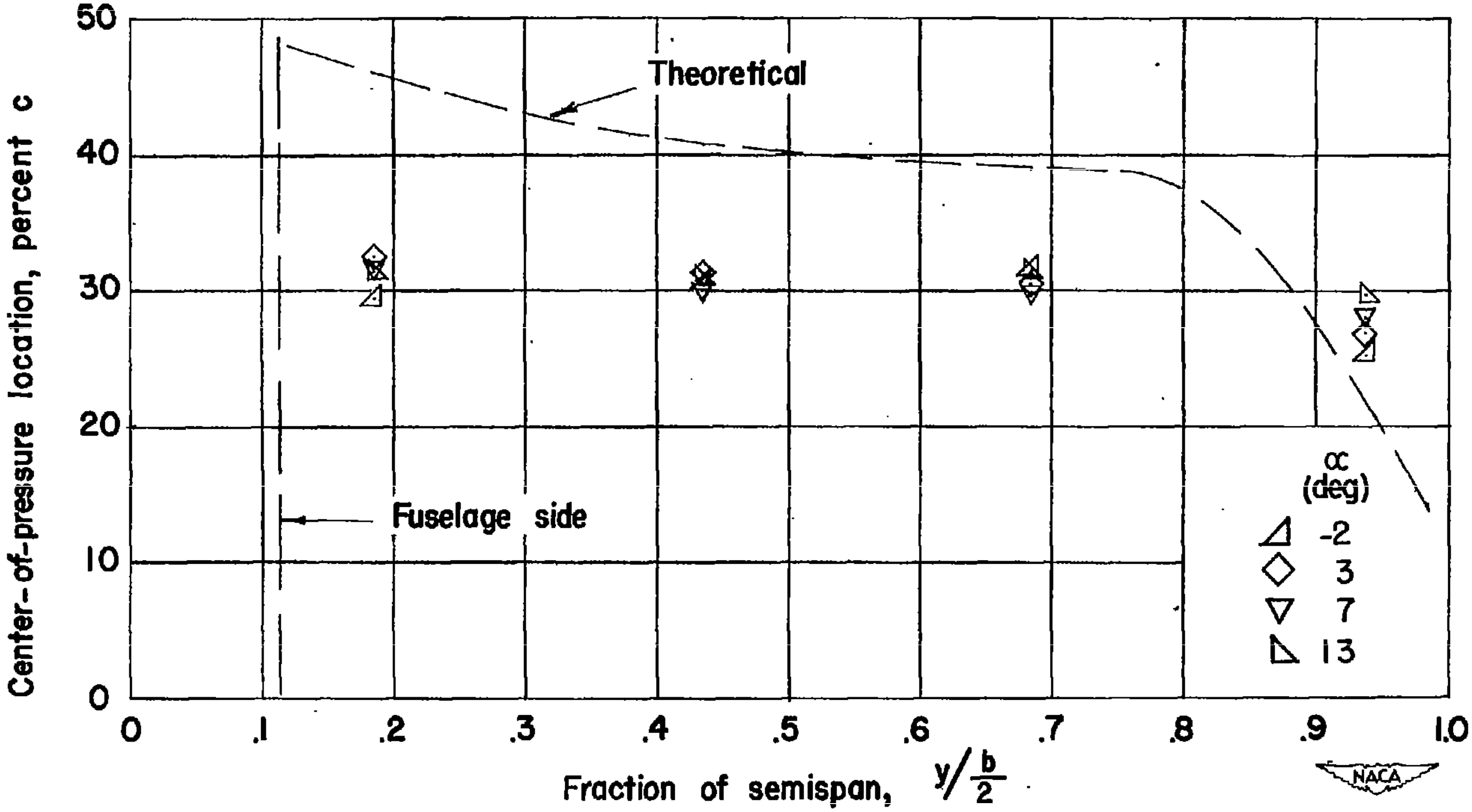

Figure 16.- Chordwise location of section center of pressure as a function of spanwise station. M = 1.40.

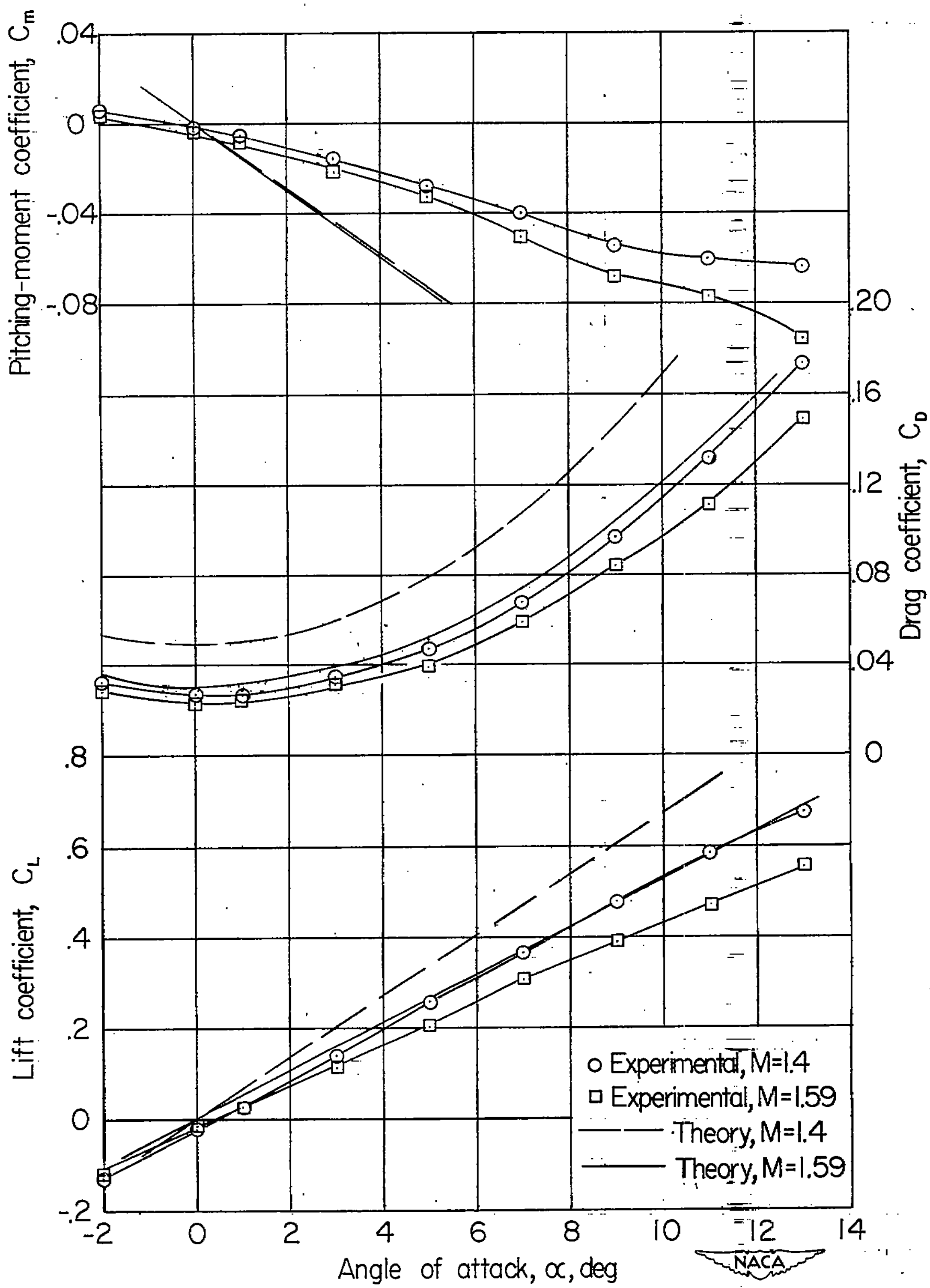

Figure 17.- Wing aerodynamic characteristics.

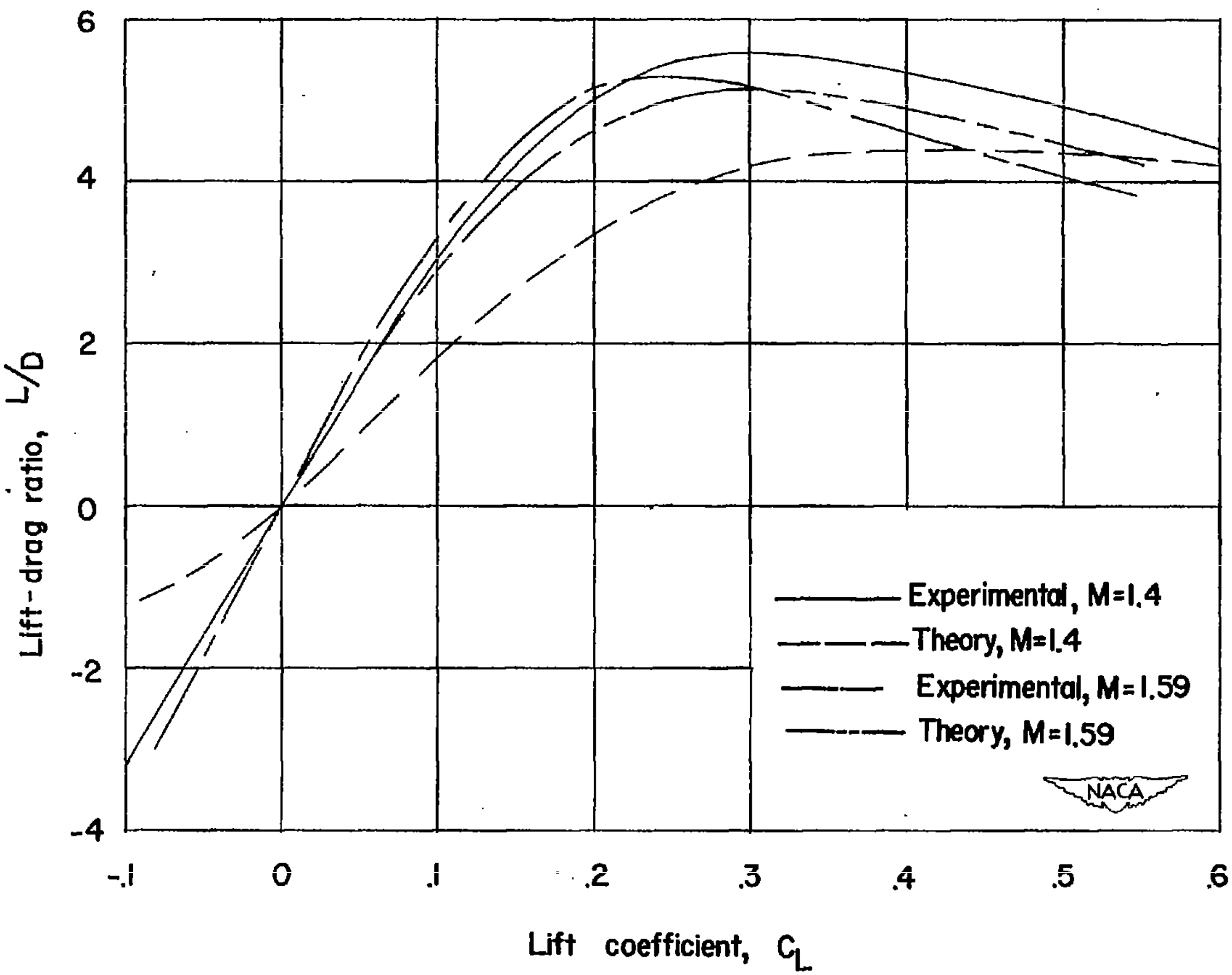

Figure 18.- Experimental and theoretical lift-drag ratios.

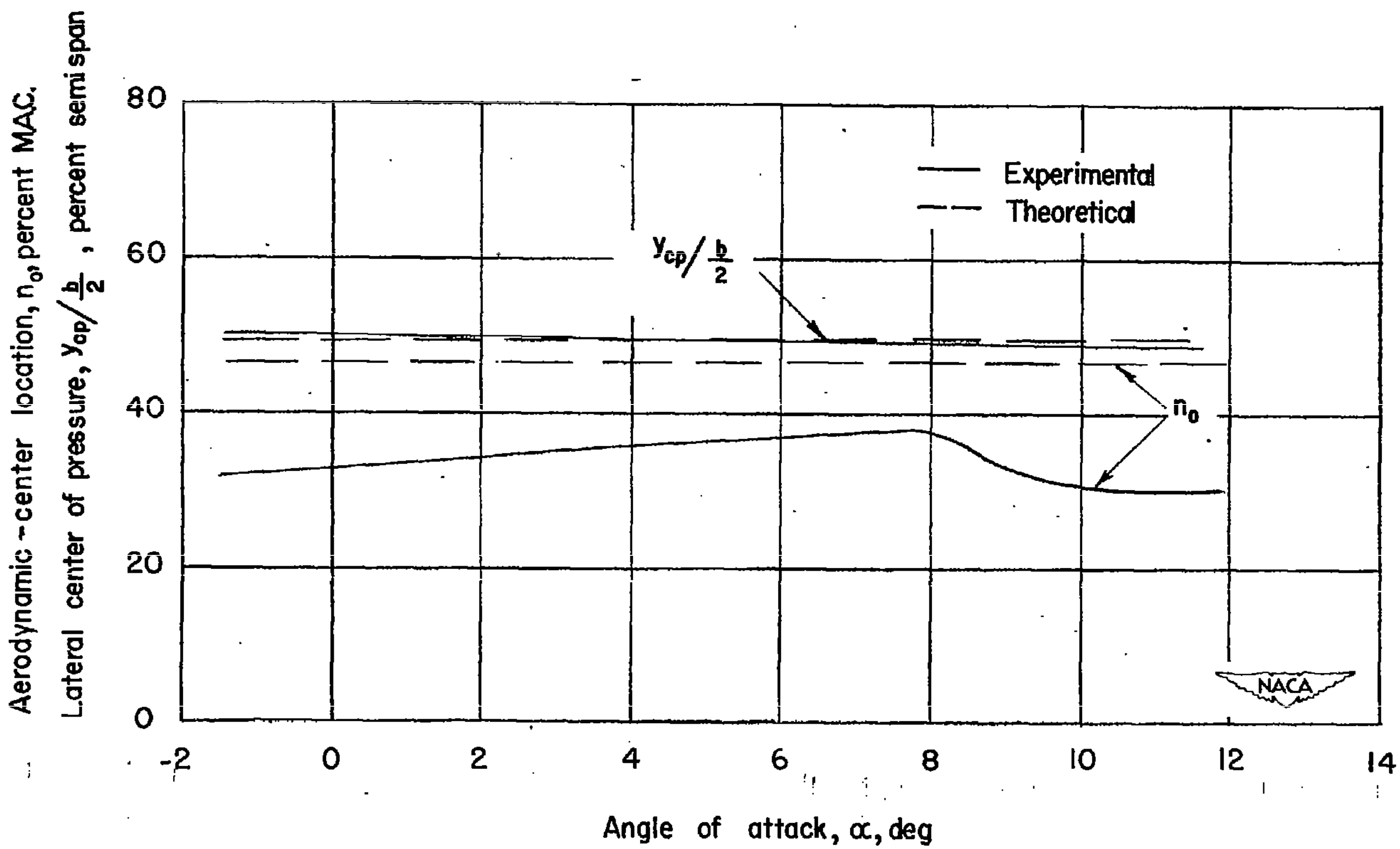

Figure 19.- Variation of aerodynamic center and lateral center of pressure with angle of attack. M = 1.40.

[redacted]

[redacted]